Draft version December 3, 2014
Preprint typeset using LaTeX style emulateapj v. 5/2/11

arXiv:1412.0695v1 [astro-ph.GA] 1 Dec 2014

AN INFRARED CENSUS OF DUST IN NEARBY GALAXIES WITH SPITZER (DUSTINGS), II. DISCOVERY OF METAL-POOR DUSTY AGB STARS

Martha L. Boyer[1,2], Kristen B. W. McQuinn[3], Pauline Barmby[4], Alceste Z. Bonanos[5], Robert D. Gehrz[3], Karl D. Gordon[6], M. A. T. Groenewegen[7], Eric Lagadec[8], Daniel Lennon[9], Massimo Marengo[10], Iain McDonald[13], Margaret Meixner[6], Evan Skillman[3], G. C. Sloan[11], George Sonneborn[1], Jacco Th. van Loon[12], Albert Zijlstra[13]

(Received; Revised; Accepted)
Draft version December 3, 2014

ABSTRACT

The DUSTiNGS survey (DUST in Nearby Galaxies with *Spitzer*) is a 3.6 and 4.5 μm imaging survey of 50 nearby dwarf galaxies designed to identify dust-producing Asymptotic Giant Branch (AGB) stars and massive stars. Using 2 epochs, spaced approximately 6 months apart, we identify a total of 526 dusty variable AGB stars (sometimes called "extreme" or x-AGB stars; $[3.6]-[4.5]>0.1$ mag). Of these, 111 are in galaxies with [Fe/H] < -1.5 and 12 are in galaxies with [Fe/H] < -2.0, making them the most metal-poor dust-producing AGB stars known. We compare these identifications to those in the literature and find that most are newly discovered large-amplitude variables, with the exception of ≈30 stars in NGC 185 and NGC 147, 1 star in IC 1613, and 1 star in Phoenix. The chemical abundances of the x-AGB variables are unknown, but the low metallicities suggest that they are more likely to be carbon-rich than oxygen-rich and comparisons with existing optical and near-IR photometry confirms that 70 of the x-AGB variables are confirmed or likely carbon stars. We see an increase in the pulsation amplitude with increased dust production, supporting previous studies suggesting that dust production and pulsation are linked. We find no strong evidence linking dust production with metallicity, indicating that dust can form in very metal-poor environments.

1. INTRODUCTION

The origin of the massive dust reservoirs in high-redshift, metal-poor quasars is under dispute ($z \lesssim 6$, $M > 10^8 M_\odot$; Bertoldi et al. 2003; Robson et al. 2004; Beelen et al. 2006). Some authors argue that core-collapse supernovae (SNe) are the dominant stellar dust source (e.g., Michałowski et al. 2010), while others argue that Asymptotic Giant Branch (AGB) stars contribute significantly (e.g., Valiante et al. 2009; Zhukovska & Henning 2013). Progenitors of core-collapse SNe produce the seeds necessary for dust production in their cores and are thus capable of producing dust at any metallicity, though it is unclear how much of the dust they produce will survive the reverse shock (e.g., Dwek et al. 2008; Kozasa et al. 2009). In AGB stars, the dust-production process is not well understood. AGB stars can be carbon- or oxygen-rich, depending on how much free oxygen is left after the dredge up of newly formed carbon; metal-poor AGB stars are more likely to be C-rich since less oxygen is available. These stars produce carbon in situ that can condense into amorphous carbon grains, but it is unclear whether the dust condensation process is limited by the metallicity of the star. AGB mass-loss models from Wachter et al. (2008) find that dust-driven mass-loss rates for solar and sub-solar metallicity carbon (C) stars are similar (down to $Z = 0.001$), but that the metal-poor stars make less dust overall. Mattsson et al. (in preparation) argue that metal-poor C stars are not a major dust source, except perhaps at the very end of their evolution.

While very dusty C stars have been observed in the Magellanic Clouds (MCs) at [Fe/H] $\gtrsim -1$ (e.g., Groenewegen & Blommaert 1998; van Loon et al. 1997, 1999, 2008; Zijlstra et al. 2006; Groenewegen et al. 2007; Lagadec et al. 2007; Gruendl et al. 2008; Riebel et al. 2012), there are few observations of similar stars at lower metallicities. Searches in nearby dwarf galaxies yield only 2 dusty C stars in Sculptor and 3 in Leo I ([Fe/H] $= -1.68$ and -1.43, respectively; Sloan et al. 2012), though these examples produce less dust (by more than an order of magnitude) than what is seen in MC stars. Using statistical arguments to estimate the size of the AGB population in several dwarf irregular galaxies (down to [Fe/H] $= -2.1$), Jackson et al. (2007a,b) and Boyer et al. (2009b) find evidence for the presence of dust-producing

[1] Observational Cosmology Lab, Code 665, NASA Goddard Space Flight Center, Greenbelt, MD 20771 USA; martha.boyer@nasa.gov
[2] Oak Ridge Associated Universities (ORAU), Oak Ridge, TN 37831 USA
[3] Minnesota Institute for Astrophysics, School of Physics and Astronomy, 116 Church Street SE, University of Minnesota, Minneapolis, MN 55455 USA
[4] Department of Physics & Astronomy, University of Western Ontario, London, ON, N6A 3K7, Canada
[5] IAASARS, National Observatory of Athens, GR-15236 Penteli, Greece
[6] STScI, 3700 San Martin Drive, Baltimore, MD 21218 USA
[7] Royal Observatory of Belgium, Ringlaan 3, B-1180 Brussels, Belgium
[8] Laboratoire Lagrange, UMR7293, Univ. Nice Sophia-Antipolis, CNRS, Observatoire de la Côte d'Azur, 06300 Nice, France
[9] ESA - European Space Astronomy Centre, Apdo. de Correo 78, 28691 Villanueva de la Cañada, Madrid, Spain
[10] Department of Physics and Astronomy, Iowa State University, Ames, IA 50011, USA
[11] Astronomy Department, Cornell University, Ithaca, NY 14853-6801, USA
[12] Astrophysics Group, Lennard-Jones Laboratories, Keele University, Staffordshire ST5 5BG, UK
[13] Jodrell Bank Centre for Astrophysics, Alan Turing Building, University of Manchester, M13 9PL, UK

stars, but were unable to identify individual stars owing to confusion with unresolved background galaxies. In this work, we identify hundreds of dusty AGB star candidates in galaxies more metal-poor than the MCs and investigate the effect of metallicity on dust production. The results have important implications for the dust budgets of high-redshift, metal-poor galaxies.

1.1. *Extreme (x-)AGB Stars*

The Surveying the Agents of Galaxy Evolution (SAGE) *Spitzer* surveys of the Small and Large Magellanic Clouds (SMC/LMC) obtained 3.6–70 μm photometry covering the full spatial extent of each galaxy, thereby detecting the circumstellar dust around the near-complete population of AGB stars in each galaxy (Meixner et al. 2006; Gordon et al. 2011). In both galaxies, a subset of AGB stars with colors $J - K \gtrsim 2$ mag show evidence for significantly more dust production than that observed for the average AGB star. Most of these stars are C-rich (Woods et al. 2011), and their mass-loss rates exceed the nuclear-burning mass consumption rate (cf. Boyer et al. 2012). These stars are sometimes referred to as "extreme" (x-)AGB stars, and we use this terminology here to be consistent with the recent work in the MCs (e.g., Blum et al. 2006).

The x-AGB stars comprise <6% of the total AGB population, but they account for more than 75% of the dust produced by cool evolved stars (Matsuura et al. 2009; Srinivasan et al. 2009; Boyer et al. 2012; Riebel et al. 2012). These stars also contribute significantly to the global 8-μm flux of the SMC (Melbourne & Boyer 2013). Other than those in the MCs and the Milky Way, x-AGB stars have been detected and their dust production confirmed in only a few galaxies: M33 (McQuinn et al. 2007; Javadi et al. 2013), M32 (Jones et al. 2014), Sgr dSph (McDonald et al. 2012), Fornax and Sculptor (Matsuura et al. 2007; Groenewegen et al. 2009; Sloan et al. 2009), so it is unclear whether AGB stars in metal-poor galaxies are efficient dust producers.

1.2. *DUSTiNGS*

Boyer et al. (2014, hereafter Paper I) describe the Dust in Nearby Galaxies with *Spitzer* (DUSTiNGS) survey in detail. DUSTiNGS is a 3.6 and 4.5 μm imaging survey of 50 nearby dwarf galaxies designed to detect all dust-producing evolved stars. Targets include 37 dwarf spheroidal (dSph), 8 dwarf irregular (dIrr), and 5 transition type (dTrans or dSph/dIrr) galaxies (see Table 1 from Paper I). The target galaxies have experienced a variety of different star formation and interaction histories and span a wide range in mass traced by visible light ($0 > M_V > 15.2$ mag) and metallicity ($-2.72 <$ [Fe/H] < -1.1).

It is difficult to separate AGB stars belonging to a galaxy from unresolved background sources and foreground stars at these wavelengths. In Paper I, we used the large field of view to estimate the size of the thermally-pulsing (TP-)AGB population by statistically estimating and removing the foreground and background sources for each galaxy, assuming that the tip of the Red Giant Branch (TRGB) is at $M_{3.6} = -6$ mag. We found that the Andromeda satellites in the sample harbor 40 ± 30 to 506 ± 48 AGB stars each (including dusty and non-dusty stars), with the largest populations in And VII, And XVIII, and And X. The most metal-poor galaxies in the sample have the lowest masses, and therefore are the least likely to harbor AGB stars. In these galaxies, we found only upper limits on the size of the AGB population (<9 each), with the exception of 20 ± 9 AGB stars in the Hercules Dwarf ([Fe/H] $= -2.41$). The largest AGB populations are in the star-forming dIrr galaxies.

In Paper I, we also found evidence for x-AGB stars in 8 of the DUSTiNGS galaxies (And II, Cetus, IC 10, IC 1613, NGC 147, NGC 185, Sextans B, and WLM), though it is impossible to isolate galaxy members from red background sources with only 3.6 and 4.5 μm imaging. In order to identify individual x-AGB stars, the DUSTiNGS images were obtained in 2 epochs, separated by approximately 6 months. Dust-producing AGB stars are expected to pulsate with periods ranging from 100–1000 days (Vassiliadis & Wood 1993), though little is known about how the mid-IR properties of these stars are affected by pulsation. Light curves for pulsating AGB stars in the MCs, the Milky Way, and in nearby dwarf spheroidal galaxies show that pulsation amplitudes decrease from optical to near-infrared (IR) wavelengths (Le Bertre 1992, 1993; Whitelock et al. 2003; Menzies et al. 2010; Battinelli & Demers 2012), but 1-20 μm light curves of Galactic AGB stars from Harvey et al. (1974) and Le Bertre (1992, 1993) suggest that amplitudes of dusty sources may increase in the IR owing to changes in the warm circumstellar dust that is responding to the pulsations of the photosphere. McQuinn et al. (2007) obtained 5 epochs of imaging of M33 with *Spitzer*, and were able to identify a large population of dust-producing C star candidates with 3.6 μm amplitudes up to 0.8 mag (amplitudes in that work are the standard deviation of over the 5 epochs). The SAGE observations of the MCs obtained 2 epochs of imaging, and find that the x-AGB stars show amplitudes up to 1.4 mag at 3.6 μm (Vijh et al. 2009; Polsdofer et al. 2014).

Here, we report the identification of 526 x-AGB star candidates in the DUSTiNGS galaxies that were discovered via their 3.6 and 4.5 μm variability, including 12 in galaxies with [Fe/H] < -2. These are the most metal-poor dust-producing AGB stars known thus far. This paper is organized as follows. In Section 2, we describe the data, stellar classification, and variability analysis. In Section 5, we compare the DUSTiNGS variables to previously detected variables and C stars in these galaxies. In Section 6, we discuss the spatial distributions, amplitudes, and dust production of the x-AGB star candidates. We summarize the results in Section 7.

2. DATA & OBSERVATIONS

To identify candidate variable AGB stars, we use the 2-epoch DUSTiNGS data and an additional epoch of data from the *Spitzer* archive from earlier programs. We use the *Spitzer* colors to identify variable stars that are producing dust.

2.1. *DUSTiNGS Data*

The DUSTiNGS observations and photometry are described in detail in Paper I. In brief, each galaxy was imaged simultaneously at 3.6 and 4.5 μm to at least the

half-light radius (r_h) in 2 epochs. The separation between epochs was determined by *Spitzer's* visibility windows for each target. The average epoch separation is 180 days, with a range of 127–240 days (Table 2 from Paper I). All photometry that we use here is from the "good-source" catalog (GSC), which has been culled to include only high-confidence point sources and reliable measurements (Paper I).

Padova stellar evolution models suggest that >90% of the TP-AGB population is brighter than the TRGB at a given time (Marigo et al. 2008, 2013, and G. Bruzual, private communication). The TRGB ranges from $M_{3.6} = -6.6$ to -6 mag, based on *Spitzer* observations of 8 dIrr galaxies (Jackson et al. 2007a,b; Boyer et al. 2009b). To ensure that the majority of the TP-AGB stars are measured, the DUSTiNGS photometry is at least 75% complete down to this limit. However, the IRAC colors and magnitudes of AGB stars make it difficult to distinguish them from foreground stars and unresolved background galaxies. This is especially true for target galaxies more distant than ≈250 kpc ($(m-M)_0 \gtrsim 22$ mag), for which individual AGB stars can be fainter than unresolved background galaxies. In Paper I, we estimated the total AGB population size by statistically subtracting the background and foreground contamination. Here, we use stellar variability to identify a subset of individual AGB candidates.

2.2. *Additional Spitzer Data*

Eight of the DUSTiNGS targets were also observed with *Spitzer* during the cryogenic mission. The observations for these galaxies are described in detail in Jackson et al. (2007a,b) and Boyer et al. (2009b). In brief, the total integration times and dithering strategies are nearly identical to DUSTiNGS, but the fields of view are significantly smaller. For 6 galaxies (Aquarius, Leo A, LGS 3, Pegasus, Phoenix, and Sextans A), only a single ≈5′×5′ IRAC frame was observed. IC 1613 was imaged in a 2×3 IRAC map and WLM in a 3×1 IRAC map (See Figs. B2 and B3). We downloaded the data from these programs (Programs 128 and 40524, P.Is.: R. D. Gehrz and E. D. Skillman, respectively), processed with the S18.25.0 pipeline, from the *Spitzer* Heritage Archive and produced photometric catalogs following the same process used for the DUSTiNGS data (Paper I).

The 3.6 μm observations for all 8 galaxies and both 3.6 and 4.5 μm observations for IC 1613 and WLM were obtained prior to 2006 (Program 128). The 4.5 μm observations for the remaining 6 galaxies were obtained in 2007 (Program 40524). See Jackson et al. (2007a,b) and Boyer et al. (2009b) for specific dates for each set of observations. Since this epoch occurs prior to the DUSTiNGS observations, we refer to it as 'epoch 0'.

3. IDENTIFYING AGB STARS

We use variability between the epochs to identify individual AGB stars and use colors and magnitudes to separate x-AGB stars from the less dusty AGB stars. Tables 1 and 2 show the total numbers of variable AGB stars in each galaxy and Table 3 includes the resulting list of classified variables.

3.1. *Color Classification*

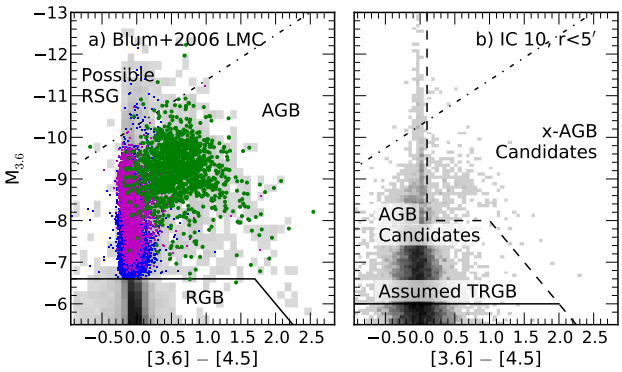

FIG. 1.— Classification of Variable Sources. *(a)* LMC Evolved Stars from Blum et al. (2006). Blue and magenta dots are less dusty oxygen-and carbon-rich AGB stars, respectively. Green dots are x-AGB stars. The greyscale includes all evolved stars, including red supergiants (RSG), AGB stars, and red giant branch (RGB) stars. Young main sequence stars are not included, but are expected to have $[3.6]-[4.5] = 0$ mag. The dashed lines show the approximate boundaries between RSG, AGB, and RGB stars. In the LMC, the TRGB is at −6.6 mag (Boyer et al. 2011). *(b)* IC 10 CMD within $r = 5'$ ($r_h = 2'.65$). The TRGB is unknown for most DUSTiNGS galaxies, so we assume it lies at −6 mag. To mimic the classification scheme used in the LMC, we classify variable sources found to the right of the dashed line as x-AGB candidates. Variable sources to the left are AGB candidates, and those below the assumed TRGB are classified as "unknown".

In the LMC, Blum et al. (2006) designate stars with colors $J-[3.6] > 3.1$ mag as x-AGB stars. This color is empirically observed as the point where there is a sudden break, or decrease in source density, in the C star sequence evident in a $J-[3.6]$ vs. [3.6] color-magnitude diagram. This break roughly corresponds to the superwind phase of AGB evolution, wherein the mass-loss rate increases dramatically due to an increase in dust production by a factor of 10 or more (Schröder et al. 1999). At low metallicities, the superwind phase may be triggered by the dredge-up of carbon (Lagadec & Zijlstra 2008). Many AGB stars not classified as x-AGB also show dust emission, though the dust emission from x-AGB stars is significantly stronger.

Most of the DUSTiNGS galaxies do not have available J-band photometry at the necessary depth to use the Blum et al. (2006) classification scheme. Instead, we mimic it based on the positions of AGB stars in the [3.6]−[4.5] CMD (Fig. 1a) and classify variables as follows:

Unknown: Variables fainter than the assumed TRGB ($M_{3.6} = -6$ mag; solid line in Fig. 1b). The TRGB is not known for most of the DUSTiNGS galaxies, but it can be as bright as $M_{3.6} = -6.6$ (Jackson et al. 2007a,b; Boyer et al. 2009b).

Less dusty AGB stars: Variables brighter than the assumed TRGB and bluer than the dashed line in Figure 1b.

x-AGB stars: Variables redder than the dashed line in Figure 1b. The luminosity limit for x-AGB stars becomes fainter at redder colors to allow for the obscuration of the dustiest sources while also avoiding the region dominated by unresolved background sources (see Paper I).

Red supergiants: AGB stars can exceed the classi-

cal AGB limit when experiencing hot-bottom burning (Boothroyd & Sackmann 1992), so variables brighter than the dot-dashed line in Figure 1 could be either massive red supergiants (RSGs) or AGB stars. We classify these stars as AGB or x-AGB depending on their color and also flag them as potential RSGs in Table 3.

Our classification scheme would correctly classify 93–94% of the Blum et al. (2006) x-AGB stars in the LMC and SMC. Similarly, <2% of other AGB types in the MCs would be mis-classified as x-AGB using our scheme.

We note that the x-AGB stars here are not the same as the very extreme AGB stars in the LMC, as defined by Gruendl et al. (2008). That work discovered 13 LMC C stars that are among the reddest objects in that galaxy ([3.6] − [4.5] up to 3.4 mag). All of the Gruendl et al. (2008) stars are so dust enshrouded that they are faint even at 3.6 μm ($M_{3.6} > -5$ mag), and are beyond the sensitivity limit of DUSTiNGS. Only one star in the DUSTiNGS sample approaches the colors of the Gruendl et al. (2008) sources: a star in IC 10 with [3.6] − [4.5] = 2.4 mag (see Section 4.2 and Fig. 1).

Unknown variable stars may be AGB stars in the minimum brightness phase of pulsation, but they could also be non-AGB variable sources such as RR Lyrae, eclipsing binaries, or background Active Galactic Nuclei (AGN). Cepheid variables are too faint at these wavelengths, so we do not expect them to contaminate the AGB sample.

3.2. *Identification of Variable Sources*

To identify individual AGB candidates, we use the variability index defined by Vijh et al. (2009):

$$V_\lambda = \frac{f_{\lambda,i} - f_{\lambda,j}}{\sqrt{\sigma f_{\lambda,i}^2 + \sigma f_{\lambda,j}^2}}, \quad (1)$$

where f_λ is the flux density of a source, σf_λ is the uncertainty in flux, and i and j indicate different epochs. Assuming a 2-dimensional Gaussian probability distribution in $V_{3.6\mu\mathrm{m}}$ and $V_{4.5\mu\mathrm{m}}$, we identify high-confidence variable star candidates as those with a joint probability falling outside $3\,\sigma$. Less confident variables stars are those falling between $2\,\sigma$–$3\,\sigma$. In both cases, candidates must show variability indices more than $2\,\sigma$ outside the mean at both 3.6 and 4.5 μm, in the same direction. We illustrate this technique for Sextans B in Figure 2.

For galaxies with a third epoch of data (Section 2.2), we computed equation 1 comparing epoch 0 to each of the DUSTiNGS epochs to identify additional variable candidates. Inclusion of epoch 0 results in 14 more 2σ and 19 more 3σ variables for these 8 galaxies, including 16 variable x-AGB candidates (Table 2). These additional variables are located in the central region of each galaxy (Fig. B1, B2, and B3).

3.2.1. *Likelihood of Detection via the Variability Index*

Because we have only 2–3 epochs, the cadence of the observations can be unfavorable for the detection of variables with particular amplitudes and periods. In general, the variability index is less sensitive to small-amplitude variable stars and stars with periods on the order of the separation between the epochs (≈180 days). To determine the "completeness" of the detected variables, we compute the probabilities of detecting variable stars with the DUSTiNGS observations for stars with periods ranging from 50–3000 days and peak-to-peak amplitudes up to 1 mag at 3.6 μm. Figure 3 shows the result of this simulation. For comparison, we also show the SMC and LMC optically-detected variable x-AGB stars (from the Optical Gravitational Lensing Experiment III, OGLE III; Udalski et al. 2008a,b). The DUSTiNGS variability index is insensitive to stars with amplitudes less than ≈0.15 mag (especially less-evolved O-rich AGB stars;

TABLE 1
Variable AGB and x-AGB Star Candidates

Galaxy	[Fe/H][c]	N_{AGB}[a] $(2\,\sigma)$	N_{AGB}[a] $(3\,\sigma)$	$N_{\mathrm{x\text{-}AGB}}$[b] $(2\,\sigma)$	$N_{\mathrm{x\text{-}AGB}}$[b] $(3\,\sigma)$
And I	-1.45 ± 0.04	0	1	0	3
And II	-1.64 ± 0.04	0	0	0	2
And V	-1.60 ± 0.30	0	1	0	0
And IX	-2.20 ± 0.20	0	0	1	4
And X	-1.93 ± 0.11	2	2	0	0
And XI	-2.00 ± 0.20	4	2	0	0
And XII	-2.10 ± 0.20	3	0	0	0
And XIII	-1.90 ± 0.20	1	1	1	0
And XIV	-2.26 ± 0.05	3	0	0	0
And XVII	-1.90 ± 0.20	0	0	1	0
And XVIII†	-1.8 ± 0.10	1	0	0	0
And XIX	-1.90 ± 0.10	1	0	0	0
And XXI	-1.80 ± 0.20	1	0	0	0
And XXII	-1.62 ± 0.05	1	1	0	0
Antlia†	-1.60 ± 0.10	3	0	0	0
Aquarius†	-1.30 ± 0.20	3	0	0	2
Cetus	-1.90 ± 0.10	1	0	1	1
CVn II	-2.20 ± 0.05	0	1	0	0
IC 10†	-1.28	13	9	18	217
IC 1613	-1.60 ± 0.20	4	4	3	27
Leo A	-1.40 ± 0.20	0	0	0	3
Leo T	-1.99 ± 0.05	0	1	0	0
LGS 3	-2.10 ± 0.22	1	1	0	1
NGC 147†	-1.10 ± 0.10	8	5	7	69
NGC 185†	-1.30 ± 0.10	5	6	4	54
Pegasus	-1.40 ± 0.20	0	0	1	5
Phoenix	-1.37 ± 0.20	0	1	0	1
Sag DIG†	-2.10 ± 0.20	0	1	0	6
Sextans A†	-1.85	1	0	1	23
Sextans B†	-1.6	1	2	4	28
Tucana	-1.95 ± 0.15	1	3	0	0
WLM	-1.27 ± 0.04	5	0	2	20

Note. — Number of variable stars within the given color-magnitude space detected at the $2\,\sigma$ and $3\,\sigma$ level (Section 3.2). This is the maximum number of variables allowing for the uncertainty in $(m - M)_0$ (see Table 1 from Paper I). The number of sources included here are confined to the spatial area covered by all epochs and wavelengths (see Table 2 from Paper I).

[a] Sources are included here if they are bluer than the dashed line in Figure 1b and brighter than $M_{3.6} = -6$ mag.

[b] Sources are included here if they are redder than the dashed line in Figure 1b.

[c] Metallicities from McConnachie (2012), also see Paper I.

† These galaxies have <75% complete photometry at $M_{3.6} = -6$ mag due either to their distance or to crowding, though all galaxies reach 75% completeness by $M_{3.6} = -6.8$ mag (Paper I). N_{AGB} should be considered a lower limit in these cases. Photometric incompleteness does not $N_{\mathrm{x\text{-}AGB}}$ except within the central ≈1′ region of IC 10 and 0.5′ in NGC 185.

TABLE 2
Number of Additional AGB Star Candidates from Epoch 0

Galaxy	$N_{\rm AGB}$ ($2\,\sigma$)	($3\,\sigma$)	$N_{\rm x\text{-}AGB}$ ($2\,\sigma$)	($3\,\sigma$)
Aquarius	0	0	0	0
IC 1613	3	2	1	3
Leo A	1	0	0	0
LGS 3	1	0	0	0
Pegasus	2	1	0	2
Phoenix	0	0	0	0
Sextans A	0	0	0	3
WLM	0	0	3	4

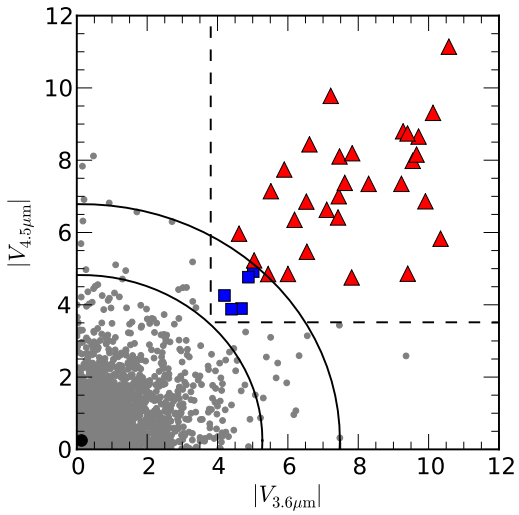

Fig. 2.— Selection of variable stars in Sextans B. The filled black circle marks the mean of the distribution. The dashed line marks the $2\,\sigma$ values for the absolute values of the variability indices at each wavelength ($|V_{3.6\mu m}|$ and $|V_{4.5\mu m}|$). Error ellipses denoting the joint probability of $2\,\sigma$ and $3\,\sigma$ are plotted as solid lines. Variable star candidates with high confidence (joint probability $>3\,\sigma$) are marked as filled red triangles. Less confident variable star candidates (joint probability $>2\,\sigma$) are marked with filled blue boxes. Table 1 lists the number of variable star candidates selected in each target galaxy.

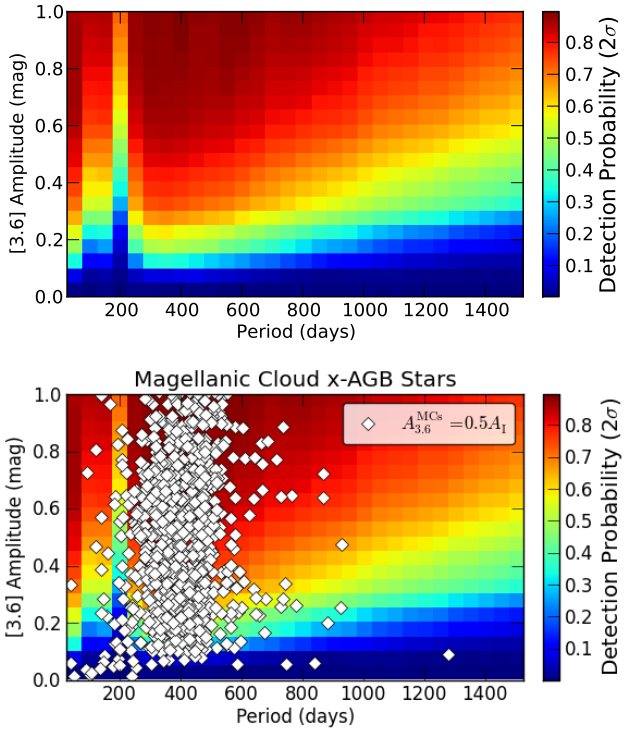

Fig. 3.— *Upper panel:* Probability of a $2\,\sigma$ detection of a variable star given a separation of 180 days (6 months) between 2 epochs. The DUSTiNGS galaxies have an epoch separation of 127–240 days (Paper I). *Lower panel:* SMC and LMC variable x-AGB stars (white diamonds). Periods and $I-$band amplitudes come from the OGLE survey (Soszyński et al. 2008). We assume that the 3.6 μm amplitude is half the I-band amplitude.

Fig. A1), but it is particularly suited to detect the x-AGB stars with periods ranging from 300–600 days.

This simulation assumes that the 3.6 μm amplitude is equal to half the I-band amplitude, since it is known that the amplitude tends to decrease at near-IR wavelengths (e.g., Whitelock et al. 2006, 2009; Menzies et al. 2008). Little is known about typical AGB star amplitudes at IRAC wavelengths; for IRC+10216, the L' (3.79 μm) amplitude is $\approx 0.75A_{\rm J}$ (Le Bertre 1992). The most extreme, optically-obscured AGB stars ($[3.6]-[4.5] \gtrsim 0.9$ mag) may be more easily detected by DUSTiNGS if they follow the general trend for more evolved stars having larger amplitudes (e.g., the C star LI-LMC 1813; van Loon et al. 2003).

3.2.2. *Contamination Among Variable Candidates*

With 2 epochs of IRAC data, spaced 3 months apart, Vijh et al. (2009) conducted a similar variability analysis for the LMC with data from the SAGE program (Meixner et al. 2006). Using additional optical and near-IR photometry, they classified sources into different types of AGB stars (carbon-rich, oxygen-rich, and x-AGB stars), using the classification scheme outlined by Blum et al. (2006). They found that the most (92%) of the variable stars detected in the LMC above the TRGB are one of these AGB types. young stellar objects (YSOs), as classified by Whitney et al. (2008), comprise 15% of the remaining variable sources. The rest were unclassified, and may include Cepheids, RR Lyrae stars, and eclipsing binaries. Based on their results, we expect non-AGB variable stars to comprise only a small percentage of the variable candidates detected in the DUSTiNGS galaxies (see Fig. A1a).

Since x-AGB stars are more evolved than regular O-rich and C-rich AGB stars, their periods are longer and their amplitudes are larger, making them the easiest stars to detect with only 2 epochs. Almost half of the variable stars detected by Vijh et al. (2009) in the LMC above the TRGB are x-AGB stars, despite the fact that these very dusty, short-lived stars comprise only 4.5% of the total LMC AGB population (Boyer et al. 2011).

It is also possible that variable sources are background AGN, which are known to vary irregularly (for a review, see Ulrich et al. 1997). Most of the known background AGN are fainter than 16 mag at 3.6 μm (e.g., Sanders et al. 2007), so we do not expect much AGN contamination among the x-AGB variable stars. In addition, even though we observe a large population of faint and red sources, few red sources fainter than the x-AGB candidates are detected as variable here. This suggests that the DUSTiNGS survey is not sensitive to AGN ampli-

TABLE 3
Variable Star Candidates

Galaxy	GSC ID[a]	α J(2000)	δ J(2000)	$\langle m_{3.6}\rangle$ (mag)	$\langle m_{4.5}\rangle$ (mag)	$\Delta m_{3.6}$[b] (mag)	$\sigma_{\rm Var}$	Type[c]	$\log \dot{D}$[c] $[M_\odot\,{\rm yr}^{-1}]$	$N_{\rm epochs}$[d]	Flag[e]	Notes[f]
LGS 3	12570	01 04 16.82	+21 51 51.0	18.95	17.93	1.33	3	A	···	2	···	···
LGS 3	27414	01 04 05.85	+21 52 39.1	19.20	18.00	0.94	2	U	···	3	E	···
LGS 3	28221	01 04 05.35	+21 50 22.3	17.28	16.79	0.74	2	A	···	2	···	···
LGS 3	47308	01 03 55.31	+21 52 47.9	15.22	14.76	0.37	3	X	−8.83	2	···	···
LGS 3	67343	01 03 43.92	+21 52 30.0	18.54	17.97	0.64	2	A	···	3	···	···
Phoenix	84555	01 51 25.22	−44 29 06.6	17.27	16.62	0.70	3	A	···	2	···	···
Phoenix	89777	01 51 23.01	−44 29 53.6	18.42	17.91	1.16	3	U	···	2	···	···
Phoenix	102714	01 51 17.81	−44 21 17.3	19.20	18.27	0.57	2	U	···	2	···	···
Phoenix	116894	01 51 12.01	−44 31 58.1	18.84	18.32	0.72	2	U	···	2	···	···
Phoenix	130056	01 51 06.56	−44 26 08.7	18.83	18.86	0.76	3	U	···	3	···	···
Phoenix	133756	01 51 05.06	−44 22 24.8	17.76	17.93	0.88	3	U	···	2	···	···
Phoenix	143442	01 51 00.97	−44 28 14.6	14.41	14.12	0.45	3	X	−9.06	2	···	Mira[e]
Phoenix	144095	01 51 00.71	−44 27 54.5	18.61	18.82	0.48	3	U	···	3	···	···
Phoenix	145317	01 51 00.21	−44 28 08.5	18.61	17.90	1.01	3	U	···	3	···	···
Phoenix	148263	01 50 58.99	−44 23 22.5	19.60	19.00	0.66	2	U	···	2	···	···
Phoenix	206620	01 50 33.63	−44 27 50.4	19.41	18.84	0.60	2	U	···	2	···	···

Note. — The variable star candidate catalog for LGS 3 and Phoenix. The catalog is available for all galaxies in the electronic version of the paper. The electronic catalog also includes magnitude and amplitude uncertainties. Stars are considered variable candidates if they are detected as variable at the 2 or 3 σ level ($\sigma_{\rm Var}$).

[a] The GSC is the "good-source catalog", described in Paper I.

[b] We define the amplitude ($\Delta m_{3.6}$) as the difference between the maximum and minimum magnitude.

[c] Stars are classified as described in Section 3.1 as x-AGB (X), AGB (A) or unknown (U). Dust-production rates ($\dot{D}$) are derived only for x-AGB candidates, and the possible $\dot{D}$ saturation limit is not applied to numbers in this table (Section 6.2).

[d] Most variable stars were found by comparing epochs 1 and 2, but some were only detected as variable by including epoch 0 (Section 2.2). For those detected via epoch 0, the mean magnitude in this table includes all 3 epochs.

[e] Variables are flagged if they lie near a bright star (B), the frame edge (E) or Column Pulldown (P). The measured fluxes may be affected in all three cases (Section 4.1). We also flag stars brighter than the dot-dash line in Fig. 1 as possible RSG stars.

[f] If a variable candidate was identified as either a long-period variable or a C star in Section 5, it is marked in this column along with its reference. In Phoenix, star #143442 is a Mira (Menzies et al. 2008).

tudes and/or cadences.

4. RESULTS

The results of the color and variable classifications are listed in Tables 1, 2, and 3. In this section, we describe the observed properties of the x-AGB variable stars.

4.1. *Variable x-AGB Star Candidates*

In the entire DUSTiNGS sample, we find 526 variable x-AGB candidates among 710 total variable sources. The number of variable AGB star candidates in each galaxy is listed in Tables 1 and 2. We quote the maximum number of AGB candidates allowing for the uncertainty in the distance moduli (Paper I). Individual variable sources are listed in Table 3 along with mean magnitudes, the lower limits on the 3.6 μm amplitude ($\Delta m_{3.6} = |m_{3.6}^{\rm epoch\,1} - m_{3.6}^{\rm epoch\,2}|$), and the classification. This table is available to download in the electronic version of this paper.

We have flagged a small subset of the variable sources listed in Table 3 that may be affected by imaging artifacts that cause the star to appear artificially variable. Some x-AGB candidates are located near imaging artifacts caused by "Column Pulldown"[14], which can be seen as lines of faint pixels emanating from bright point sources. This affects 11 variable x-AGB star candidates in And IX, And XIII, Aquarius, IC 10, NGC 147, Sag DIG, and Sextans A. In addition, some variable sources fall on the edge of the spatial coverage ($\lesssim$10″ from the edge) where fewer frames contribute to the total depth owing to frame dithering (Paper I). There are fewer frames to assist in the elimination of imaging artifacts in these regions, which may affect the measured fluxes. This affects 4 variable x-AGB candidates, including 2 in And IX, 1 in IC 1613, and 1 in IC 10. We also checked whether proximity to a bright star might affect the measured flux and found 1 variable x-AGB star in

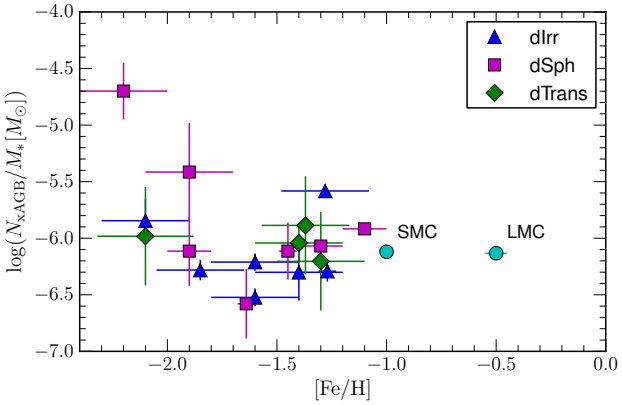

Fig. 4.— The number of x-AGB variable candidates normalized to the total stellar mass as a function of metallicity. Masses and metallicities are from McConnachie (2012) and are listed in Paper I. Y-axis error bars reflect Poisson uncertainties only. The square in the upper left is And IX, but imaging artifacts may affect 3 of the 5 x-AGB variables in this galaxy (see Section 4.1). This plot includes only variables detected from epochs 1 and 2 to avoid artificial inflation of the number of variables detected in the subset of galaxies with epoch 0 data.

[14] http://irsa.ipac.caltech.edu/data/SPITZER/docs/irac/iracinstrumenthandbook/home/

NGC 147 that may be artificially variable. We exclude affected sources from further analysis, with the exception of source #21181 in And IX at α(J2000) = $13^{\rm h}18^{\rm m}54\overset{\rm s}{.}04$, δ(J2000) = $+43°12'2\overset{''}{.}8$. This star may be marginally affected by Column Pulldown at 3.6 μm in epoch 2 and 4.5 μm in epoch 1, but since the color is similar between epochs and the amplitude at each wavelength is similar, we include it in the analysis as a high-confidence x-AGB star.

In Paper I, we estimated the total size of the x-AGB population by statistically subtracting the foreground and background sources. For the 6 galaxies with large x-AGB populations and firm (non-upper-limit) estimates from Paper I, the fraction of x-AGB stars detected as variable ranges from 33%–61% (this includes IC 10, IC 1613, NGC 147, NGC 185, Sextans B, and WLM). Using the AGB star catalogs for the LMC and SMC from Boyer et al. (2011) and the OGLE I-band periods, we find that a DUSTiNGS-like survey would detect ≈62% of the OGLE-detected MC x-AGB stars (probability of a 2-σ detection >0.75 with 1000 trials; Section 3.2.1). The difference in detection fractions is more likely a reflection of the differences in the distance to a galaxy and the epoch separation, and not to a real difference in the pulsation amplitudes between galaxies. A more distant galaxy has larger photometric uncertainties resulting in a lower probability of detection, and a longer epoch separation results in a higher probability of detection, in general.

Figure 4 shows the total number of x-AGB variable candidates, normalized to each galaxy's total stellar mass, as a function of metallicity, using the masses and metallicities from McConnachie (2012). There is no clear metallicity trend for the number of x-AGB stars in a galaxy, suggesting that the dominant factor determining the number of x-AGB stars is the star formation history.

4.2. *Color-Magnitude Diagram*

In Paper I, we showed that the CMDs for most of the DUSTiNGS galaxies are dominated by foreground and/or background sources, making it difficult to see the true color distribution of AGB stars. In Figure 5, we show the location of the variable candidates overplotted on the CMD, separated by the morphological type of the galaxy. The greyscale in panels *a*–*c* is the average background-subtracted CMD for all 50 galaxies. For comparison, Figure 5d includes a similar diagram with the variables identified in the LMC by Vijh et al. (2009, see Section 3.2.2). We detect few blue AGB stars compared to the LMC, though x-AGB stars are recovered at a similar rate. This is due to dustless stars pulsating with amplitudes that are smaller than the DUSTiNGS photometric uncertainty (Fig. A1).

Most of the x-AGB star candidates with $[3.6]-[4.5] \gtrsim 1.5$ mag are in IC 10, which by far harbors the largest x-AGB population (Table 1) and is thus the most likely to be host to rarer stellar types. Otherwise, only one star each from Sextans B, NGC 185, and NGC 147 is as red as the IC 10 x-AGB stars (Fig. 5). With the exception of NGC 147 and NGC 185, the dSph galaxies harbor few examples of x-AGB candidates, as expected based on their star formation histories. Altogether, we find only 10 x-AGB star candidates in the remaining 35 dSph galaxies. Star #21181 in And IX is particularly red (Fig. 5c), indicating strong dust production (Section 6.2).

The variable x-AGB candidates are most likely C-rich AGB stars, as is indicated in the MCs (e.g., Woods et al. 2011; Riebel et al. 2012). However, a small fraction might be O-rich, especially the brightest examples near the RSG border in Figure 1a where hot-bottom burning might disrupt the dredge-up of carbon. It is impossible to distinguish the different chemistries without near-IR photometry or spectra (Section 5.2).

4.3. *Spatial Distributions*

Most of the x-AGB variable stars are confined to within 1–2 half-light radii ($r_{\rm h}$; Figs. B1–B3). However, in some galaxies the x-AGB stars can be found at large radii (e.g., IC 10). In Sextans B, x-AGB stars fill the full DUSTiNGS coverage (≈$13' \times 14'$). This is much more extended than the small half-light radius listed in McConnachie (2012) ($r_{\rm h} = 0\overset{'}{.}9$), and agrees better with the new estimate from Bellazzini et al. (2014) of $r_{\rm h} = 1\overset{'}{.}9$.

As in the LMC and SMC (Blum et al. 2006; Sandstrom et al. 2009; Boyer et al. 2011), the x-AGB star distributions are generally smooth and symmetric, with a few exceptions. In Sextans B, the x-AGB stars beyond the half-light radius are preferentially located to the north, which may be due to the influence of Sextans A and NGC 3109, which are located nearby and towards the south. In Sextans A, x-AGB stars are to the southwest of the center, avoiding the region of star formation on the east side of the galaxy. NGC 185 is lacking x-AGB stars to its north and south, despite the almost circular distribution of other stellar types in the galaxy. In IC 10, the x-AGB candidates avoid a region of strong star formation just to the southeast of the galaxy's center, which may be due in part to crowding (Paper I). Finally, in NGC 147 there is a lack of AGB stars on the southeast side of the galaxy. A detailed examination of the radial distribution of x-AGB stars in each galaxy will be presented in a forthcoming paper.

4.4. *IR Amplitudes*

In general, pulsation amplitudes increase with periods (e.g., Vassiliadis & Wood 1993; Whitelock et al. 2000). Thus, amplitudes will increase as a star evolves, and larger amplitudes may thus be linked with more dust formation. With only two or three epochs, we can present only a lower-limit amplitude for each variable star ($\Delta m = |m^{\rm epoch\,1} - m^{\rm epoch\,2}|$; Table 3). The mean $\Delta m_{3.6}$ detected for x-AGB stars is 0.50 ± 0.23 mag (standard deviation). Using the variable catalog from Vijh et al. (2009) in the LMC, we compute that the same $\Delta m_{3.6}$ for 820 x-AGB stars in the LMC is 0.36 ± 0.19 mag. The lower LMC mean amplitude is probably due to the smaller distance to the LMC. As a result, photometric uncertainties in the LMC data are smaller and enable the detection of smaller amplitudes.

The maximum amplitude is for a star in Sextans B ($\Delta m_{3.6} = 1.6$ mag) that has a mean color of $[3.6]-[4.5] = 0.61$ mag and is located on the outskirts of the galaxy (upper right of Fig. B2 at α(J2000)= $09^{\rm h}59^{\rm m}46\overset{\rm s}{.}07$, δ(J2000)= $+05°26'08\overset{''}{.}8$). The amplitude of this star is similar to the largest $\Delta m_{3.6}$ detected for an x-AGB star in the LMC ($\Delta m_{3.6}^{\rm max} = 1.8$ mag). Since amplitudes tend to decrease with wavelength for long-period variables

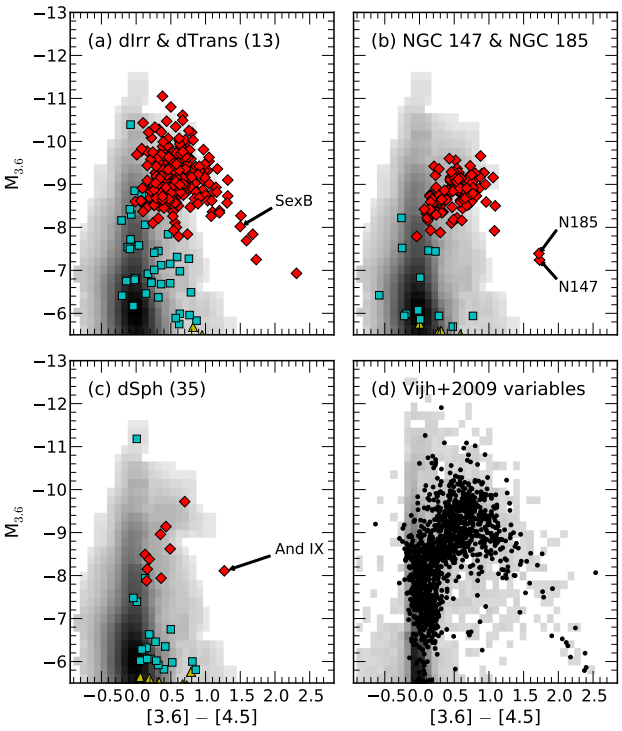

FIG. 5.— Location of variable sources on the CMD. The x-AGB variable star candidates are plotted as red diamonds, AGB variable star candidates as cyan squares, and unknown variables as yellow triangles. The greyscale background in all panels is the mean background-subtracted CMD (plotted as the density of sources) for all 50 target galaxies. *(a):* Variable sources from the 13 dIrr and dTrans galaxies. All x-AGB stars redder than $[3.6]-[4.5] = 1.5$ mag are in IC 10, except the one star labeled Sextans B. *(b):* Variable sources from NGC 147 and NGC 185, which we plot separately since they dominate the dSph x-AGB populations. *(c):* Variable sources from the remaining 35 dSph galaxies. *(d):* Variable sources detected with 2 epochs separated by 3 months in the LMC (Vijh et al. 2009), plotted over the same greyscale background shown in Figure 1a.

(e.g., Le Bertre 1992), the large amplitudes detected in some DUSTiNGS stars may imply amplitudes of several magnitudes in the optical. An alternate explanation is that the large IR amplitude is the result of a varying temperature of warm circumstellar dust. Since 3.6 μm may be measuring the Wien tail of the dust blackbody, even small changes in the total dust opacity or temperature could result in large changes at 3.6 μm. Changes in the strength of molecular absorption features (possibly from dust veiling) might also account for amplitude changes with wavelength.

In Figure 6, we show $\Delta m_{3.6}$ for each variable x-AGB star as a function of the host galaxy's metallicity. There is no clear trend indicating a change in pulsation properties in metal-poor environments.

Figure 6 also shows $\Delta m_{3.6}$ as a function of color. Even with only 2 epochs, it is evident that the amplitude tends to increase with $[3.6]-[4.5]$. This trend supports a direct link between the star's pulsation and the dust production, and adds to evidence of the same link seen in the Galaxy, M33, and Sgr dSph variable AGB stars (Whitelock et al. 2006; McQuinn et al. 2007; McDonald et al. 2014).

The difference between the 3.6 and 4.5 μm amplitudes of x-AGB stars is small, with $\langle \Delta m_{3.6} - \Delta m_{4.5} \rangle = 0.02 \pm 0.11$ mag. There is no trend for a systematic increase or decrease in the amplitudes from 3.6 to 4.5 μm.

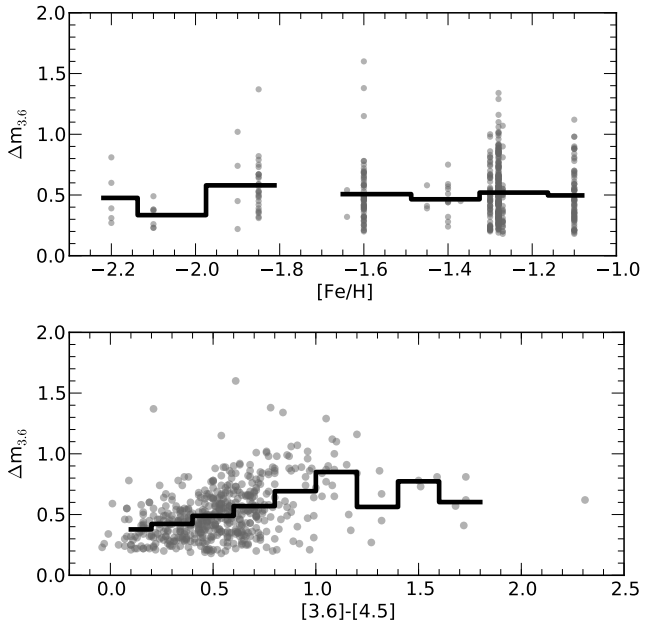

FIG. 6.— IR amplitudes of x-AGB variables. Dots in these diagrams are transparent; regions that appear darker gray thus indicate a higher density of points. *Top Panel:* The minimum amplitude as a function of metallicity. The histogram marks the mean of the plotted points within the given metallicity bin. The mean 2-epoch minimum amplitude of LMC x-AGB stars from Vijh et al. (2009) is 0.36 mag at 3.6 μm. *Bottom Panel:* Amplitude as a function of $[3.6]-[4.5]$, with the mean amplitude within color bins marked by the solid line. Even with only 2 epochs, a trend for increasing color with amplitude is clear. McQuinn et al. (2007) see a similar trend in M33 at the same wavelengths. There is no strong trend linking color and metallicity (see Fig. 12).

5. PREVIOUSLY DETECTED AGB STARS

The red colors and variability of DUSTiNGS x-AGB candidates support the strong likelihood that they are true dust-producing AGB stars. However, with only 2 epochs of 3.6 and 4.5 μm imaging, they remain candidates. In this section, we cross-identify the DUSTiNGS sources with existing optical and near-IR surveys to confirm some of the x-AGB candidates as C stars and/or long-period variables (LPVs).

5.1. *Comparison to Known Variables*

All TP-AGB stars are LPVs ($20 \lesssim P \lesssim 1000$ days), pulsating regularly or semi-regularly during different phases of their evolution (e.g., Fraser et al. 2008; Soszyński et al. 2009). At the end of their evolution, AGB stars become Miras, which pulsate in the fundamental mode and generally have red colors, large amplitudes, and periods longer than 100 days (Iben & Renzini 1983). Miras and other LPVs have previously been detected in only 4 of the DUSTiNGS galaxies: NGC 147, NGC 185, IC 1613, and Phoenix.

5.1.1. *NGC 147 and NGC 185*

Lorenz et al. (2011) (hereafter, L+11) searched for LPVs in NGC 147 and NGC 185 with 30 epochs of photometry in the i-band. They found 182 and 387 LPVs, respectively, that are also detected in the K_S-band. Their

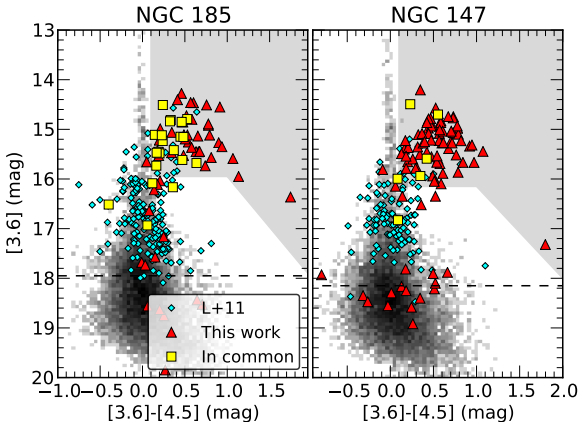

FIG. 7.— LPVs from Lorenz et al. (2011). Variable sources in common between this work and L+11 are marked with yellow squares. The shaded area marks the region used to identify x-AGB candidates and the dashed line marks the assumed location of the TRGB.

survey includes stars within $R \sim 3.5'$, or about half the radius probed with DUSTiNGS. We find only 6 variables in common with NGC 147 and 22 with NGC 185. The i-band amplitudes measured by L+11 are ≈0.2–2 mag. Since we have detected only a small fraction of the L+11 LPVs, it follows that the amplitudes of the stars covered by L+11 are significantly smaller at 3.6 μm than in the i-band, on average. For the variable stars detected both here and by L+11, the mean amplitudes are 0.5 mag larger in the i-band than at 3.6 μm ($\langle A_i \rangle = 0.9$ mag and $\langle A_{3.6} \rangle = 0.4$ mag).

Nowotny et al. (2003) used narrow-band photometry centered on the TiO and CN bands to distinguish O-rich from C-rich AGB stars in NGC 147 and NGC 185 (also see Section 5.2). In NGC 185, the 24 L+11 LPVs detected as variable here include 5 O-rich stars (M type), 5 C-rich stars, and 4 stars with C/O ≈ 1 (S type). Most of the M stars that are also LPVs in L+11 are within 2 mag of the assumed TRGB, but of the 5 M stars that are detected as variable here, 4 are bright and red enough to be classified as x-AGB variables. This suggests that these 4 stars may be massive enough to undergo hot-bottom burning. Similarly, in NGC 147, we detect 2 M type, 3 C-rich, and 1 S type star. One of these M-type LPVs is quite bright at $M_{3.6} = -9.7$ mag and may therefore be a massive AGB star or a red supergiant.

Figure 7 shows the DUSTiNGS CMD for these galaxies with L+11 variables marked. It is clear that optical and near-IR surveys are biased against the reddest sources that are uncovered by DUSTiNGS. This also suggests that red LPVs have larger pulsation amplitudes at 3.6 μm than bluer LPVs (Section 4.4). Within the same coverage surveyed by L+11, we detect 38 and 28 new variable star candidates in NGC 147 and NGC 185. Of these, most are x-AGB candidates.

5.1.2. *IC 1613*

Kurtev et al. (2001) (hereafter K+01) detected one M-type Mira in IC 1613 at α(J2000) = $1^h04^m48^s.97$, δ(J2000) = $+2°05'28''.8$. This star is also detected here as a 3σ variable with $\langle m_{3.6} \rangle = 14.63$ mag and $\langle [3.6] - [4.5] \rangle = 0.16$ mag, which qualifies it as an x-AGB candidate. K+01 measured a period of 641 d and an R-band amplitude >2.5 mag. The lower limit on the 3.6 μm amplitude measured here is $\Delta m_{3.6} = 0.43$ mag.

Several works (most recently, Antonello et al. 2000; Mantegazza et al. 2001; Dolphin et al. 2001) have searched for variable stars in IC 1613, focusing on short-period Cepheids and RR Lyr stars. K+01 is the first to report the detection of a Mira. Here, we detect 50 new variable AGB candidates, of which 34 are x-AGB candidates.

5.1.3. *Phoenix*

Menzies et al. (2008) reported a single Mira in Phoenix (their star #51) with a period of 425 d and an amplitude of $\Delta K_S = 0.76$ mag. Its spectral type is unknown, though Menzies et al. (2008) argued it is C-rich based on its $J - K_S$ color. Here, this star is a 3σ x-AGB variable candidate with $\langle m_{3.6} \rangle = 14.41$ mag and $\langle [3.6] - [4.5] \rangle = 0.29$ mag. Its lower-limit amplitude is $\Delta m_{3.6} = 0.45$ mag.

Gallart et al. (2004) identified 5 additional LPV candidates. Menzies et al. (2008) studied two of these and found that they are not variable. One of these 5 is not detected in DUSTiNGS despite falling inside the DUSTiNGS spatial coverage. Of the remaining 4 LPV candidates, none are detected as variable here, though their colors and magnitudes suggest that they are possible AGB stars. One ($1^h50^m47^s.07$, $-44°27'43''.0$) shows $[3.6]-[4.5] = 1.0$ mag and $M_{3.6} = -7.28$ mag, suggesting that it could be a dusty AGB star.

5.2. *Comparison to Known Carbon Stars in the x-AGB Sample*

Carbon stars form more easily at low metallicity since less free oxygen is available to tie up newly formed carbon into CO molecules. Analysis of the IR spectra and spectral energy distributions (SEDs) has revealed that most of the x-AGB stars in the LMC and SMC are C-rich (Woods et al. 2011, Ruffle et al., in preparation), and it follows that C stars produce the majority of the AGB dust budget. Several of the DUSTiNGS galaxies have been observed using optical narrow-band CN/TiO photometry or JHK photometry to identify C stars. The near-IR JHK photometry is less precise than CN/TiO photometry, though at subsolar metallicities, the stars with red $J-K$ colors can be classified as high-confidence C stars (Cioni et al. 2006; Aringer et al. 2009; Boyer et al. 2013).

Neither method is sensitive to the dustiest stars because of circumstellar extinction at optical and near-IR wavelengths. Optical photometry can detect stars as red as $[3.6] - [4.5] \approx 0.5$ mag, while the reddest DUSTiNGS star detected via $J - K$ color has $[3.6] - [4.5] = 0.9$ mag (a star in Sag DIG, see below). Altogether, we confirm 70 variable x-AGB candidates as C stars. These stars are flagged in Table 3.

5.2.1. *NGC 185*

Nowotny et al. (2003) (hereafter N+03) obtained narrow-band CN/TiO photometry of NGC 185 and find 154 C stars. We detect 93 of the N+03 C stars, which have a mean color $\langle [3.6] - [4.5] \rangle = 0.05$ mag. Of these 93, 22 would be classified as x-AGB candidates based on their DUSTiNGS photometry ($([3.6] - [4.5])_{\rm max} = 0.53$ mag).

Among the DUSTiNGS variable x-AGB stars, N+03 classified 11 as C-rich, 3 as O-rich, and 3 as "other", where "other" indicates that the star did not show strong CN or TiO. Similarly, 2 DUSTiNGS variable AGB stars are classified as C-rich, and one as "other".

Battinelli & Demers (2004b) also used narrow-band CN/TiO optical filters to identify C stars in NGC 185, though they choose a slightly different CN/TiO index cut-off to classify the stars. From their C star catalog, we find 3 additional variable x-AGB candidates that are classified as C-rich for a total of 14 C-rich variable x-AGB stars in NGC 185.

5.2.2. *NGC 147*

N+03 also obtained narrow-band CN/TiO photometry in NGC 147. They find 146 C stars, of which we detect 102 in DUSTiNGS with $\langle[3.6]-[4.5]\rangle = -0.01$ mag. The blue colors of some C stars may be due absorption from CO and/or C_3 at 4–6 μm. Only 7 of the N+03 stars are x-AGB variable stars here: these have a maximum $[3.6]-[4.5] = 0.72$ mag. Of these 7 variable x-AGB stars, N+03 identified 4 as C-rich, 1 as O-rich, and 2 as "other".

Battinelli & Demers (2004a) also used CN/TiO to identify C stars in NGC 147. In addition to those classified by N+03, 13 more variable x-AGB candidates are classified as C-rich.

Sohn et al. (2006) obtained JHK photometry of stars in NGC 147 and classified an additional 10 variable x-AGB stars as C-rich. These stars have $1.95 < J-K < 3.41$ and $0.16 < [3.6]-[4.5] < 0.79$ mag. Altogether, 27 variable x-AGB stars have been classified as C-rich based on previous surveys.

5.2.3. *IC 10*

Demers et al. (2004) obtained narrow-band CN/TiO photometry of IC 10 and find 676 C stars, of which 356 are detected here with $\langle[3.6]-[4.5]\rangle = -0.09$ mag. Only 31 of these 356 C stars fall in the x-AGB region of the CMD, the reddest of which has $[3.6]-[4.5] = 0.53$ mag. Of the 235 variable x-AGB stars detected here, 13 are classified as C-rich.

IR spectra of 9 dusty O-rich stars in IC 10 were obtained by Lebouteiller et al. (2012) using *Spitzer*. None of these sources are variable in DUSTiNGS. These stars are brighter than the x-AGB candidates ($m_{3.6} \approx 13$ mag), but they show similar colors to the x-AGB stars ($0.2 < [3.6]-[4.5] < 0.5$ mag).

Magrini et al. (2003) identified 16 planetary nebulae in IC 10. Only one (PN7) is potentially detected in the DUSTiNGS images, though blending with nearby sources caused it to be excluded from the "good-source" catalog (see Paper I). Because of this, it is not included in the variability analysis here.

5.2.4. *Other Galaxies*

IC 1613: Carbon stars were identified via CN/TiO narrow-band photometry by Albert et al. (2000). They found 195 C stars, of which 107 are detected here with $\langle[3.6]-[4.5]\rangle = -0.01$ mag and 10 are in the x-AGB region of the CMD. Only one of these C stars is identified as an x-AGB variable star here.

Pegasus dIrr: Battinelli & Demers (2000) found 40 C stars using narrow-band CN/TiO photometry. 31 are detected here and 3 are variable x-AGB candidates.

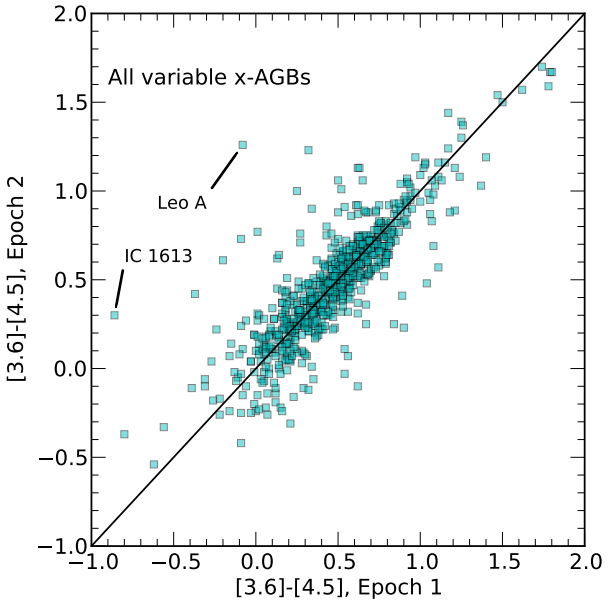

FIG. 8.— Comparison between [3.6]−[4.5] from epoch 1 to epoch 2 (≈6 month separation) for all variable x-AGB stars. The standard deviation in the color change is 0.19 mag. The solid black line marks equal colors.

Aquarius: Battinelli & Demers (2000) found 3 C stars with CN/TiO photometry. None of these are variable here, but one is in the x-AGB region of the CMD. Gullieuszik et al. (2007) found 10 C stars using JHK photometry. We detect 8 of these stars, but none are variable in DUSTiNGS. This includes 2 LPV candidates, which have $M_{3.6} = -9.67$ and -8.65 mag and $[3.6]-[4.5] = 0.62$ and 0.3 mag. Their $J-K$ colors are 2.86 and 2.01 mag, respectively.

Sag DIG: Demers & Battinelli (2002) identified 16 C stars with CN/TiO photometry. We detect 13 here, but only one is a variable x-AGB candidate. Gullieuszik et al. (2007) identified C stars via JHK photometry, and 3 are variable x-AGB candidates here. These stars have $1.74 < J-K < 4.15$ mag. These 4 stars are the first dust-producing high-confidence C stars at [Fe/H] < -2, though spectroscopy is required for definitive classification as C rich. There are 11 additional confirmed C stars that are not detected as variable here, but do fall within the x-AGB region of the CMD (Section 6.3).

WLM: Battinelli & Demers (2004c) used CN/TiO photometry to identify 149 stars. Of these, we detect 121 in DUSTiNGS and 11 are variable x-AGB candidates.

Leo A: Magrini et al. (2003) identified a planetary nebula is also detected in DUSTiNGS with $\langle[3.6]\rangle = 16.72$ mag and $\langle[3.6]-[4.5]\rangle = 1.14$ mag. This source falls on the border of the x-AGB region of the CMD, though is not detected as variable.

6. DISCUSSION

6.1. *Changes in the Dust*

Changes in the color of a dusty star over time indicate changes in the temperature and/or the optical depth of the dust. Between the epoch 1 and epoch 2 observations,

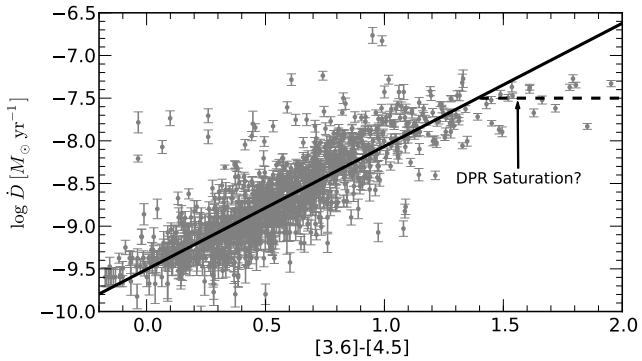

FIG. 9.— Dust-production rates (DPRs) for LMC x-AGB stars, from SED fitting to GRAMS models (Riebel et al. 2012). The solid line is the best fit (Eq. 2) and the dashed line marks the possible point of saturation in the dust-production rate, which is not applied to stars here.

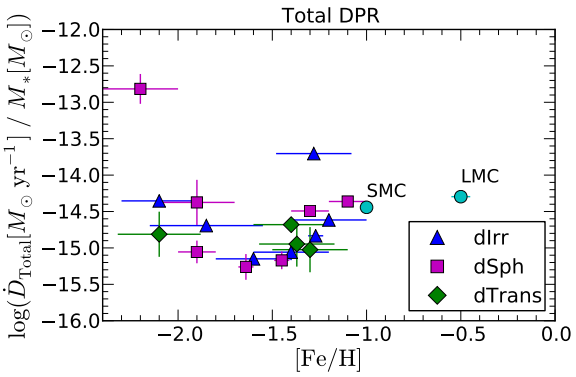

FIG. 10.— Total dust-production rate (DPR) normalized to the total stellar mass within each galaxy as a function of the galaxy's metallicity. Here, we apply the DPR saturation limit shown in Figure 9 for the reddest stars (also see Fig. 11). Only variable x-AGB stars are included in the DUSTiNGS points. LMC and SMC points were derived using the same color-criteria from the SAGE data (Meixner et al. 2006; Gordon et al. 2011), and include all x-AGB stars.

the colors of the x-AGB variable stars do not change significantly (Fig. 8), suggesting that the pulsations within a cycle do not have a strong effect on the dust on a short timescale. Comparisons in the color between epoch 0 (Section 2.2) and the DUSTiNGS epochs is not possible because the 3.6 and 4.5 μm observations are not simultaneous in epoch 0.

A subset of x-AGB variables do show a significant color change between epochs; two of these stars are marked in Figure 8. We cannot disentangle the effects of temperature and dust mass on the color of these stars with only the DUSTiNGS data. Nonetheless, it is clear that in some of the x-AGB variable stars, the circumstellar environment is changing, sometimes significantly, over a short timescale, implying that dust formation is not continuous and smooth over the dust-producing phase.

A blue $[3.6]-[4.5]$ color is typical for a less dusty C star that has CO+C_3 molecular absorption from 4–6 μm, but this feature becomes veiled as the dust emission increases (van Loon et al. 2008; Boyer et al. 2011). There are a handful of stars that appear blue in epoch 1 and red in epoch 2, suggesting that new dust appeared after the epoch 1 observations. These stars may have undergone an episode of eruptive dust production, perhaps owing to the influence of a binary companion. Further monitoring at IR wavelengths could confirm such phenomena.

6.2. *Dust Production*

Riebel et al. (2012) measured the dust produced by the entire LMC AGB population by fitting the full SEDs from the optical to the IR using the Grid of RSG and AGB modelS (GRAMS; Sargent et al. 2011; Srinivasan et al. 2011). GRAMS assumes a grain mixture of 90% amorphous carbon and 10% SiC with optical constants from Zubko et al. (1996) and Pégourié (1988), respectively, and a standard KMH grain size distribution (Kim et al. 1994). Using the catalog from Riebel et al. (2012), we find that most of stars with $[3.6]-[4.5] > 0.1$ mag are C-rich and that their dust-production rates ($\dot{D}$) increase with the color as (Fig. 9):

$$\log \dot{D}[M_\odot\,\mathrm{yr}^{-1}] = -9.5 + [1.4 \times ([3.6]-[4.5])]. \quad (2)$$

We apply this relationship to the x-AGB variable star candidates in the DUSTiNGS galaxies to get a first estimate of their total dust production, using an average between the epoch 1 and 2 colors (Section 6.1). For stars redder than $[3.6]-[4.5] \approx 1.5$ mag, the GRAMS dust-production rate appears to saturate at a $\log \dot{D} \sim -7.5$ [$M_\odot$ yr^{-1}]. We do not apply this saturation limit to the rates reported in Table 3, but we do apply it in Figure 10 and in the right panel of Figure 11. If real, this saturation limit applies to 8 x-AGB variables total in Sextans B, NGC 147, NGC 185, and IC 10 (Fig. 5).

We caution that the use of different optical constants and/or the assumption of a different wind outflow velocity (GRAMS assumes 10 km s^{-1}) could result in dust-production rates that differ by up to a factor of 10. Therefore, rates reported here are not absolutely accurate and should only be compared to rates measured using similar assumptions. We assume that these parameters do no change from galaxy to galaxy.

Figure 10 shows the total dust production, normalized to the total stellar mass, from the variable x-AGB candidates as a function of metallicity. For the LMC and SMC points, we used the SAGE catalog to select x-AGB stars using the same selection criteria used here for DUSTiNGS galaxies. We note that the LMC and SMC points include the entire x-AGB population, while the DUSTiNGS points include only the x-AGB stars detected as variable (Section 3.2.1). The total dust output shows significant scatter and does not appear to be strongly affected by metallicity. The magenta square in the upper left corner belongs to And IX, and is totally dominated by a single x-AGB variable. This star (#21181) is marginally affected by imaging artifacts (Section 4.1), so its dust-production rate may be inflated. Except for this And IX star, no other x-AGB stars that may be affected by imaging artifacts are included in this plot or in Figure 11.

In Figure 11, each point indicates the mean (or the maximum) dust-production rate among the variable x-AGB stars within one of the galaxies. While the mean $\dot{D}$ is similar at all metallicities, the maximum $\dot{D}$ may show a slight preference for more metal-rich galaxies. However, the five galaxies with the highest maximum $\dot{D}$ (LMC, SMC, IC 10, NGC 147, and NGC 185) all have the largest

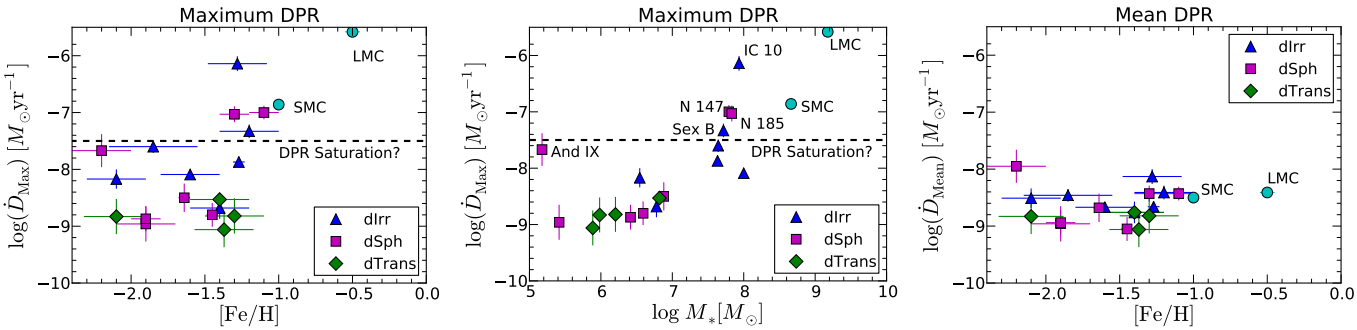

FIG. 11.— *Left:* Maximum dust-production rate (DPR) among the variable x-AGB stars within each galaxy as a function of metallicity. The point of possible DPR saturation (Fig. 9) is not applied here but is marked by a dashed line. *Middle:* The 6 galaxies with the largest $\dot{D}_{\rm max}$ are also the most massive galaxies in the sample: LMC, SMC, IC 10, NGC 185, NGC 147, and Sextans B. *Right:* Mean DPR (with the DPR saturation limit applied to the reddest stars) among the variable x-AGB stars within each galaxy, as a function of metallicity.

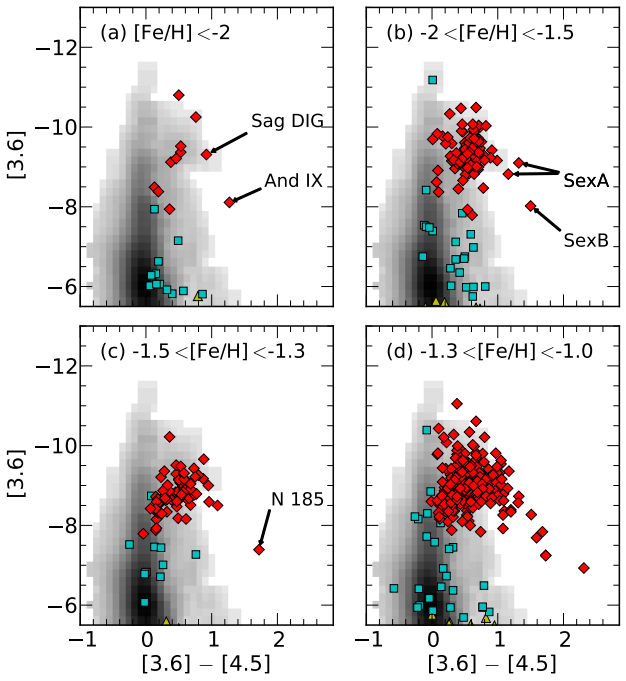

FIG. 12.— Location of variable sources on the CMD, separated by [Fe/H]. The x-AGB variable star candidates are plotted as red diamonds, AGB star candidates as cyan squares, and other variables as yellow triangles. The greyscale background in all panels is the mean background-subtracted CMD (plotted as the density of sources) for all 50 target galaxies. All x-AGB candidates in *(d)* redder than [3.6] – [4.5] = 1.5 mag are from NGC 147 and IC 10.

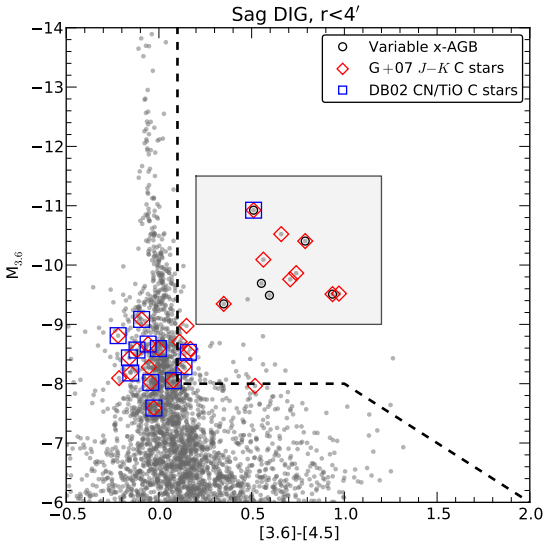

FIG. 13.— CMD of the central 4′ of Sag DIG showing high confidence x-AGB candidates within the grey box. Those detected as variable are circled in black. Sources that are confirmed C stars based on CN/TiO narrow-band photometry are marked with blue boxes (DB02; Demers & Battinelli 2002). Sources that are likely C stars based on their $J-K$ colors are marked with red diamonds (G+07; Gullieuszik et al. 2007). All sources to the right of the black dashed line are x-AGB candidates.

x-AGB populations, so are less affected by stochastics and are therefore more likely to harbor the rarest, very dusty x-AGB stars.

6.3. *Dust at Very Low Metallicity*

In globular clusters, dust-producing AGB stars have potentially been detected down to [Fe/H] = −2.4 (e.g., Boyer et al. 2006, 2008, 2009a; McDonald et al. 2009, 2011a,b; Sloan et al. 2010). These stars are low-mass ($M \lesssim 1\ M_\odot$), oxygen-rich stars that will not ultimately contribute much to the total dust budget of a galaxy (e.g., Zhukovska & Henning 2013; Schneider et al. 2014). Searches for more massive metal-poor dust-producing AGB stars have yielded few examples in Local Group dwarf galaxies (Sloan et al. 2012). The most metal-poor example is Mag 29 in Sculptor dSph ([Fe/H] = −1.68 and log $\dot{D}$ $[M_\odot\ {\rm yr}^{-1}] = -8.21$; Sloan et al. 2009), though Sloan et al. (2012) estimate that its metallicity may be as high as [Fe/H] = −1. We find a total of 111 variable x-AGB stars with [Fe/H] < −1.5 and 12 with [Fe/H] < −2, suggesting that carbon formed in and around the stellar

TABLE 4
ADDITIONAL X-AGB CANDIDATES WITH [Fe/H] < −2

Galaxy	GSC ID	RA (J2000)	Dec (J2000)	⟨[3.6]⟩ (mag)	⟨[4.5]⟩ (mag)
Sag DIG	34625	19 30 03.25	−17 41 33.6	15.84	14.86
Sag DIG	36867	19 30 02.01	−17 40 19.3	15.49	14.75
Sag DIG	38522	19 30 01.11	−17 39 59.1	15.59	14.88
Sag DIG	41056	19 29 59.76	−17 41 04.9	15.26	14.70
Sag DIG	44334	19 29 57.94	−17 40 17.3	14.82	14.16
Sag DIG	50071	19 29 54.74	−17 41 04.4	15.94	15.44
LGS 3	68695	01 03 43.01	+21 50 45.4	14.73	14.11

NOTE. — High likelihood x-AGB candidates in Sag DIG and LGS 3 that are not detected as variable in DUSTiNGS, but are located in the shaded region of Fig. 13.

core is successfully dredged up and condensed into carbon grains at all metallicities.

We assume here that the wind expansion velocity and the dust properties are the same in all the DUSTiNGS galaxies, but this assumption may not be valid. For example, Wachter et al. (2008) find that the expansion velocity decreases from solar metallicity to SMC metallicity when the ratio C/O is fixed in their models. However, Wachter et al. (2008) also find that when models are given the same absolute abundance of free carbon, the SMC-, LMC-, and solar-metallicity models have similar expansion velocities and dust-condensation efficiency. The DUSTiNGS findings support this scenario.

We show the CMD of x-AGB variable star candidates as a function of metallicity in Figure 12. The sources in Sag DIG, And IX, and LGS 3 ([Fe/H] < -2) are of particular interest, as they indicate that AGB stars can produce large amounts of dust even in the early, metal-poor Universe. The AGB models from Marigo et al. (2013) indicate that C stars can form at least as early as 10^8 yr at these metallicities ($M_{\rm initial} \sim 5\ M_{\odot}$), and perhaps even earlier depending on the details of the interplay between dredge-up and hot-bottom burning. AGB stars must therefore contribute significantly to the large dust reservoirs discovered in distant quasars (Bertoldi et al. 2003; Robson et al. 2004; Beelen et al. 2006).

Sag DIG contains the largest very metal-poor x-AGB population ([Fe/H] $= -2.1$), with 17 stars that are either x-AGB variables or confirmed C stars within the x-AGB region of the CMD (Section 5.2.4). There is one additional unconfirmed source that nonetheless has colors similar to the confirmed x-AGB stars and is within $4'$ of the galaxy center (Fig. 13). We consider this source to be a likely x-AGB star. Similarly, LGS 3 contains one additional possible x-AGB star along with the one that was identified as variable. These likely x-AGB stars are listed in Table 4.

No variable x-AGB stars were discovered in the most metal-poor DUSTiNGS galaxies ([Fe/H] < -2.2: UMa II, Segue I, Leo IV, Coma Berenices, Bootes I, or Hercules). These galaxies have very low masses ($M_{\rm V} > -6.6$ mag; for comparison And IX has $M_{\rm V} = -8.1$ mag) and show no evidence of recent star formation (Paper I and McConnachie 2012), so it is not surprising that they are lacking examples of intermediate-aged AGB stars in general. In Paper I, we estimated the size of the AGB population after subtraction of foreground and background sources. In Hercules, we estimated a total of 20 ± 9 AGB stars, which is the smallest detected AGB population among the DUSTiNGS galaxies. In the other 4 very metal-poor galaxies, we found only upper limits.

6.4. *Implications for Dust in the Interstellar Medium*

If AGB stars can efficiently produce dust at any metallicity as the DUSTiNGS data suggests, it follows that the dust-to-gas ratios (DGRs) in the (C-rich) stellar envelopes may be similar at all metallicities when the stars are in the dust-producing "superwind" phase (Habing 1996; Groenewegen et al. 2007). This implies that the DGR in the interstellar medium (ISM) should also be independent of metallicity if AGB stars are the dominant source of interstellar dust and dust grains are minimally processed after leaving the circumstellar envelope. Observations of nearby galaxies show a clear correlation between metallicity and DGR in the ISM (e.g., Galametz et al. 2011; Sandstrom et al. 2013; Fisher et al. 2014), suggesting that AGB dust may be quickly destroyed or shattered (cf. Temim et al. 2014). The remnants of grain destruction/shattering may then provide the seeds for grain accretion in molecular clouds.

7. CONCLUSIONS

We use 2-epoch 3.6 and 4.5 μm photometry to identify 710 variable sources in a sample of 50 nearby dwarf galaxies that were observed by the DUSTiNGS survey (Paper I). Among these variable sources, 526 have $[3.6] - [4.5] > 0.1$ mag colors that roughly correspond to the "extreme" (x-)AGB stars detected in the Magellanic Clouds, which have been shown to dominate the total AGB dust production in those galaxies. We find these x-AGB variable stars in 32 of the DUSTiNGS galaxies, with metallicities ranging from $-2.2 <$ [Fe/H] < -1.1. Previous optical and near-IR surveys classified 70 of these x-AGB variable stars as confirmed C stars.

Of the 526 x-AGB variables identified, 12 are in galaxies with [Fe/H] < -2.0. These include 4 known C stars in the very metal-poor galaxy Sag DIG ([Fe/H] $= -2.1$), which we have found to be the most metal-poor confirmed dust-producing C stars known.

The 2-epoch minimum amplitudes of the variable x-AGB candidates indicate an increase in amplitude with color, supporting a link between dust production and pulsation. The mean amplitudes show no variation with metallicity.

We use the $[3.6] - [4.5]$ color to estimate the dust-production rates of the x-AGB candidates, and we find that the mean dust-production rate among the x-AGB stars within any galaxy is independent of metallicity. This trend holds even when including the Large and Small Magellanic Clouds, suggesting that dust production occurs in C stars with similar efficiency at any metallicity down to at least [Fe/H] $= -2.2$. The maximum dust-production rate within a given galaxy may show a trend with metallicity. However, this trend is more likely due to a sample bias wherein the most massive galaxies that are more likely to contain the rarest dusty sources are also the galaxies with the highest metallicities.

We thank Patricia Whitelock & Michael Feast for discussions about stellar variability that improved the paper and the referee for helpful comments. This work is supported by *Spitzer* via grant GO80063 and by the NASA Astrophysics Data Analysis Program grant number N3-ADAP13-0058. MLB is supported by the NASA Postdoctoral Program at the Goddard Space Flight Center, administered by ORAU through a contract with NASA. RDG was supported by NASA and the United States Air Force. AZB acknowledges funding by the European Union (European Social Fund) and National Resources under the "ARISTEIA" action of the Operational Programme "Education and Lifelong Learning" in Greece.

REFERENCES

Albert, L., Demers, S., & Kunkel, W. E. 2000, AJ, 119, 2780

Antonello, E., et al. 2000, A&A, 363, 29

Aringer, B., et al. 2009, A&A, 503, 913
Battinelli, P. & Demers, S. 2000, AJ, 120, 1801
—. 2004a, A&A, 418, 33
—. 2004b, A&A, 417, 479
—. 2004c, A&A, 416, 111
—. 2012, A&A, 544, A10
Beelen, A., et al. 2006, ApJ, 642, 694
Bellazzini, M., et al. 2014, A&A, 566, A44
Bertoldi, F., et al. 2003, A&A, 406, L55
Blum, R. D., et al. 2006, AJ, 132, 2034
Boothroyd, A. I. & Sackmann, I. 1992, ApJ, 393, L21
Boyer, M. L., et al. 2013, ApJ, 774, 83
—. 2008, AJ, 135, 1395
—. 2009a, ApJ, 705, 746
—. 2014, ApJS, in press (Paper I)
—. 2009b, ApJ, 697, 1993
—. 2012, ApJ, 748, 40
—. 2011, AJ, 142, 103
—. 2006, AJ, 132, 1415
Cioni, M., et al. 2006, A&A, 448, 77
Demers, S. & Battinelli, P. 2002, AJ, 123, 238
Demers, S., Battinelli, P., & Letarte, B. 2004, A&A, 424, 125
Dolphin, A. E., et al. 2001, ApJ, 550, 554
Dwek, E., et al. 2008, ApJ, 676, 1029
Fisher, D. B., et al. 2014, Nature, 505, 186
Fraser, O. J., Hawley, S. L., & Cook, K. H. 2008, AJ, 136, 1242
Galametz, M., et al. 2011, A&A, 532, A56
Gallart, C., et al. 2004, AJ, 127, 1486
Gordon, K. D., et al. 2011, AJ, 142, 102
Groenewegen, M. A. T. & Blommaert, J. A. D. L. 1998, A&A, 332, 25
Groenewegen, M. A. T., Lançon, A., & Marescaux, M. 2009, A&A, 504, 1031
Groenewegen, M. A. T., et al. 2007, MNRAS, 376, 313
Gruendl, R. A., et al. 2008, ApJ, 688, L9
Gullieuszik, M., et al. 2007, A&A, 475, 467
Habing, H. J. 1996, A&A Rev., 7, 97
Harvey, P. M., et al. 1974, ApJS, 27, 331
Iben, Jr., I. & Renzini, A. 1983, ARA&A, 21, 271
Jackson, D. C., et al. 2007a, ApJ, 656, 818
—. 2007b, ApJ, 667, 891
Javadi, A., et al. 2013, MNRAS, 432, 2824
Jones, O., et al. 2014, MNRAS, in press
Kim, S.-H., Martin, P. G., & Hendry, P. D. 1994, ApJ, 422, 164
Kozasa, T., et al. 2009, in Astronomical Society of the Pacific Conference Series, Vol. 414, Cosmic Dust - Near and Far, ed. T. Henning, E. Grün, & J. Steinacker, 43
Kurtev, R., et al. 2001, A&A, 378, 449
Lagadec, E. & Zijlstra, A. A. 2008, MNRAS, 390, L59
Lagadec, E., et al. 2007, MNRAS, 376, 1270
Le Bertre, T. 1992, A&AS, 94, 377
—. 1993, A&AS, 97, 729
Lebouteiller, V., et al. 2012, A&A, 546, A94
Lorenz, D., et al. 2011, A&A, 532, A78
Magrini, L., et al. 2003, A&A, 407, 51
Mantegazza, L., et al. 2001, A&A, 367, 759
Marigo, P., et al. 2013, MNRAS, 434, 488
—. 2008, A&A, 482, 883
Matsuura, M., et al. 2009, MNRAS, 396, 918
—. 2007, MNRAS, 382, 1889
McConnachie, A. W. 2012, AJ, 144, 4
McDonald, I., et al. 2011a, ApJS, 193, 23
—. 2009, MNRAS, 394, 831
—. 2011b, MNRAS, 417, 20
—. 2012, MNRAS, 427, 2647
—. 2014, MNRAS, 439, 2618
McQuinn, K. B. W., et al. 2007, ApJ, 664, 850
Meixner, M., et al. 2006, AJ, 132, 2268
Melbourne, J. & Boyer, M. L. 2013, ApJ, 764, 30
Menzies, J., et al. 2008, MNRAS, 385, 1045
Menzies, J. W., et al. 2010, MNRAS, 406, 86
Michałowski, M. J., et al. 2010, A&A, 522, A15
Nowotny, W., et al. 2003, A&A, 403, 93
Pégourié, B. 1988, A&A, 194, 335
Polsdofer, E., et al. 2014, ApJ, in press
Riebel, D., et al. 2012, ApJ, 753, 71
Robson, I., et al. 2004, MNRAS, 351, L29
Sanders, D. B., et al. 2007, ApJS, 172, 86
Sandstrom, K. M., et al. 2009, ApJ, 696, 2138
—. 2013, ApJ, 777, 5
Sargent, B. A., Srinivasan, S., & Meixner, M. 2011, ApJ, 728, 93
Schneider, R., et al. 2014, MNRAS, 442, 1440
Schröder, K.-P., Winters, J. M., & Sedlmayr, E. 1999, A&A, 349, 898
Sloan, G. C., et al. 2010, ApJ, 719, 1274
—. 2012, ApJ, 752, 140
—. 2009, Science, 323, 353
Sohn, Y.-J., et al. 2006, A&A, 445, 69
Soszyński, I., et al. 2008, AcA, 58, 163
Soszyński, I., et al. 2009, AcA, 59, 239
Srinivasan, S., et al. 2009, AJ, 137, 4810
Srinivasan, S., Sargent, B. A., & Meixner, M. 2011, A&A, 532, A54
Temim, T., et al. 2014, ApJ, in press
Udalski, A., et al. 2008a, AcA, 58, 89
—. 2008b, AcA, 58, 329
Ulrich, M.-H., Maraschi, L., & Urry, C. M. 1997, ARA&A, 35, 445
Valiante, R., et al. 2009, MNRAS, 397, 1661
van Loon, J. Th., et al. 2008, A&A, 487, 1055
—. 1999, A&A, 351, 559
—. 2003, MNRAS, 341, 1205
—. 1997, A&A, 325, 585
Vassiliadis, E. & Wood, P. R. 1993, ApJ, 413, 641
Vijh, U. P., et al. 2009, AJ, 137, 3139
Wachter, A., et al. 2008, A&A, 486, 497
Whitelock, P., Marang, F., & Feast, M. 2000, MNRAS, 319, 728
Whitelock, P. A., et al. 2006, MNRAS, 369, 751
—. 2003, MNRAS, 342, 86
—. 2009, MNRAS, 394, 795
Whitney, B. A., et al. 2008, AJ, 136, 18
Woods, P. M., et al. 2011, MNRAS, 411, 1597
Zhukovska, S. & Henning, T. 2013, A&A, 555, A99
Zijlstra, A. A., et al. 2006, MNRAS, 370, 1961
Zubko, V. G., et al. 1996, MNRAS, 282, 1321

APPENDIX

A. DETECTION PROBABILITIES OF OTHER VARIABLE SOURCES

Figure A1 shows the detection probability (Section 3.2.1) of other types of variable stars with DUSTiNGS.

B. SPATIAL DISTRIBUTION OF VARIABLE X-AGB CANDIDATES

Figures B1, B2 and B3 show the *Spitzer* 3.6 μm maps of galaxies with variable x-AGB candidates.

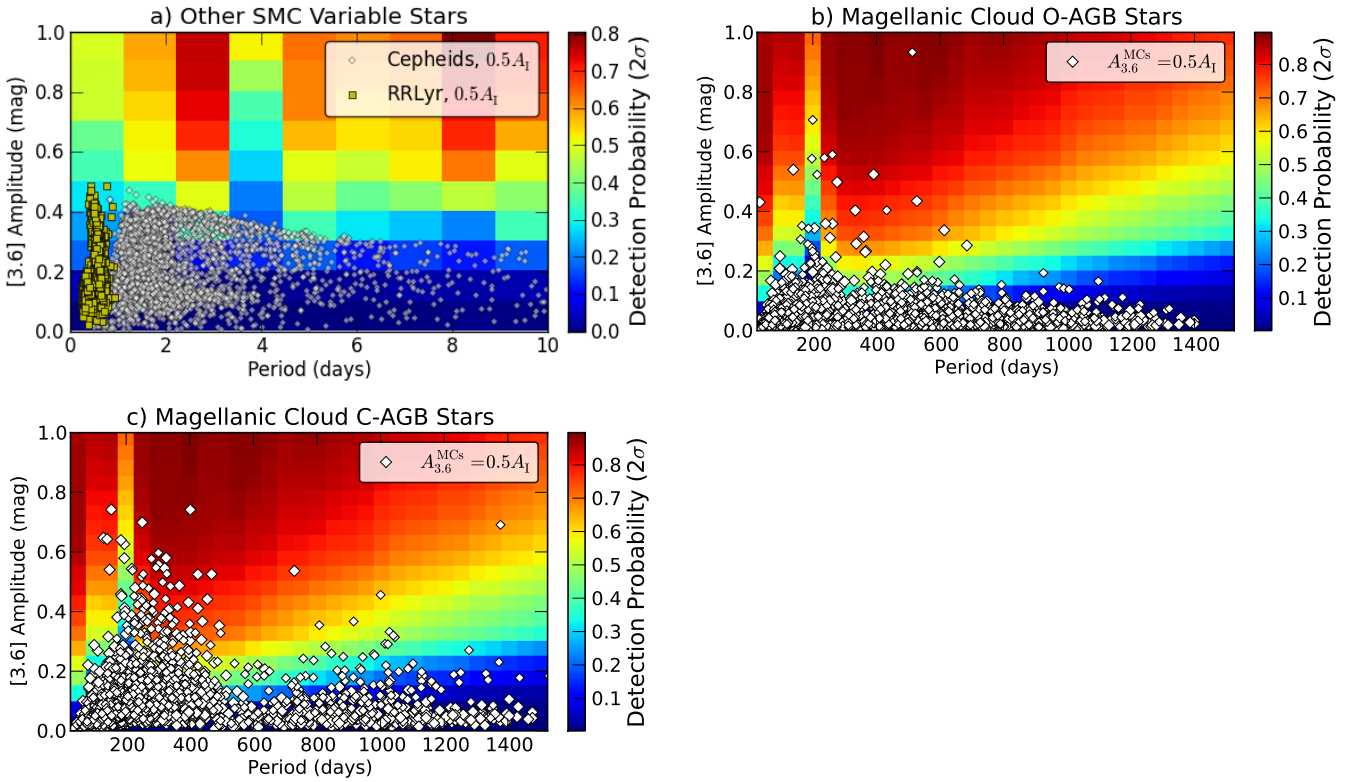

FIG. A1.— Probability of detecting *a)* Cepheid and RR Lyr variable stars, *b)* O-rich AGB stars with $[3.6]-[4.5]<0.1$ mag, and *c)* C-rich AGB stars with $[3.6]-[4.5]<0.1$ mag. In all three panels, the white and yellow points are variables detected by the OGLE survey (Soszyński et al. 2008) in the Magellanic Clouds by the I-band amplitudes and periods. The distribution in the detection probability in panels *b)* and *c)* is identical to that in Figure 3. AGB identification is from the SAGE Survey (Boyer et al. 2011). Cepheids and RR Lyr shown in *a)* are included regardless of their brightness; most stars of this type are fainter than the TRGB.

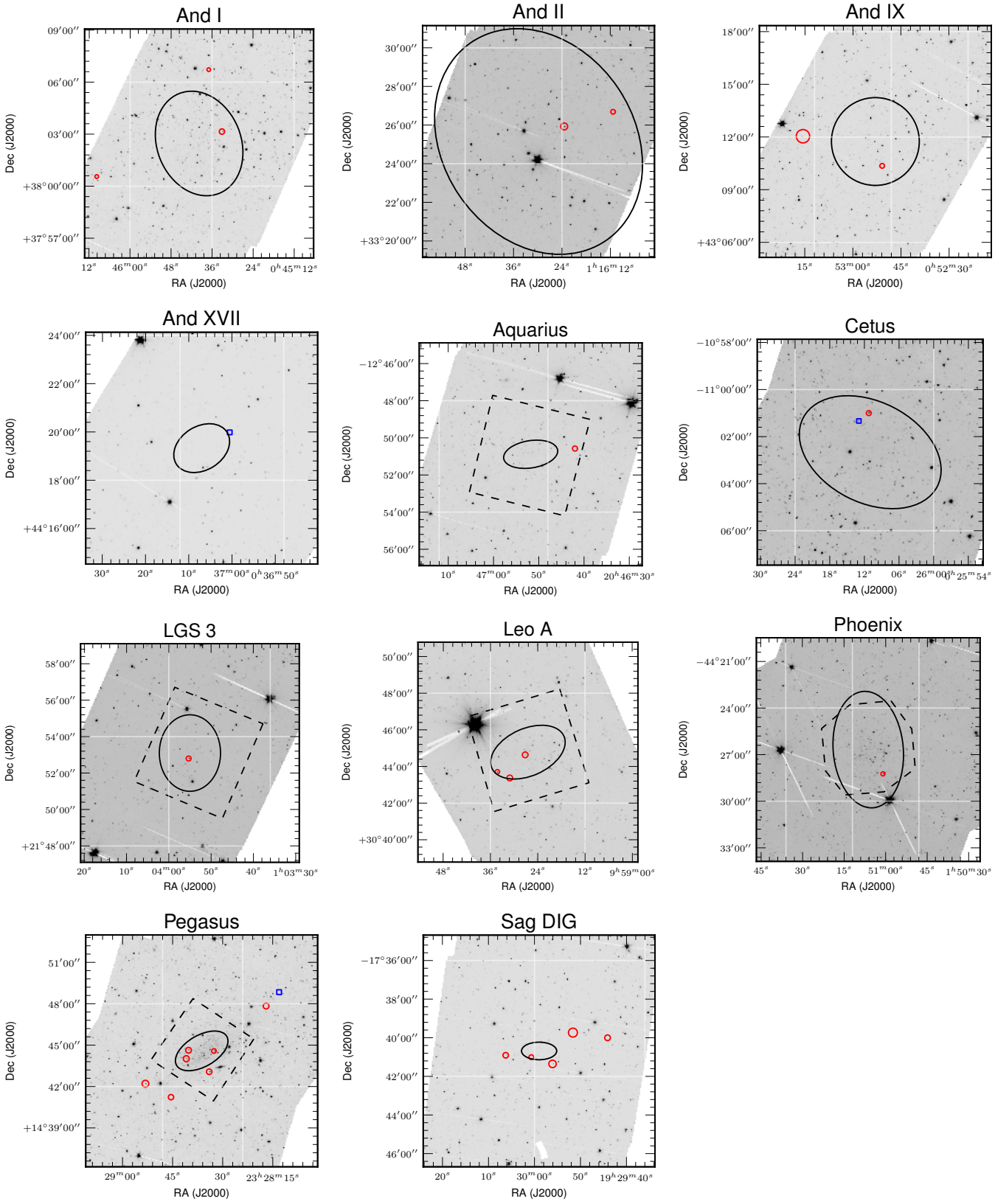

FIG. B1.— Spatial location of x-AGB variable candidates. Red circles are 3-σ variables, blue squares are 2-σ variables. The size of the symbol is representative of the [3.6] − [4.5] color, with larger symbols representing redder colors. The half-light radii are marked with black ellipses. And IX has unknown ellipticity (McConnachie 2012), so we plot a circular half-light radius. Dashed lines marks the epoch 0 coverage. The x-AGB stars that may be affected by imaging artifacts (Table 3) are not included except the very red star (#21181) in And IX.

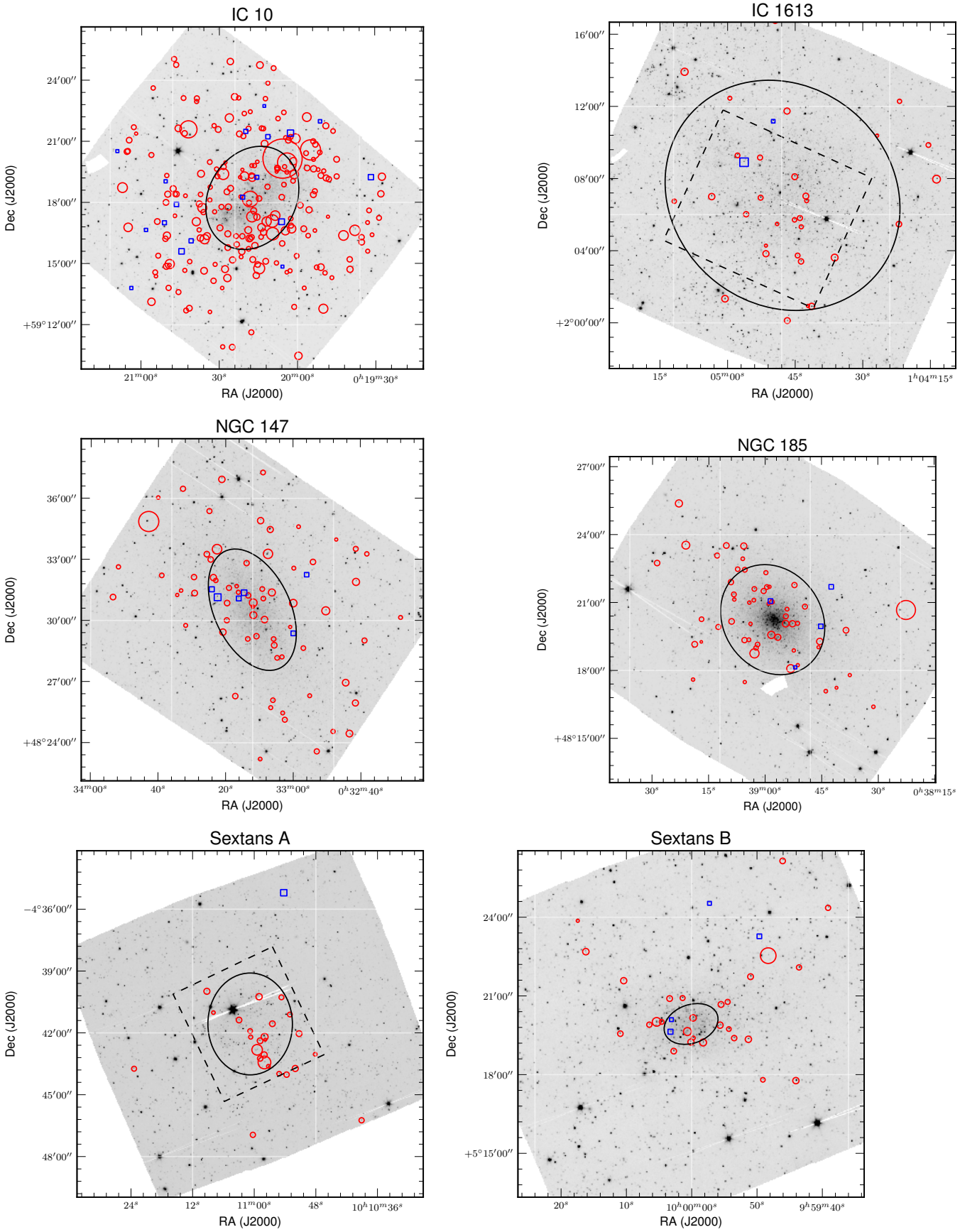

FIG. B2.— Figure B1 continued.

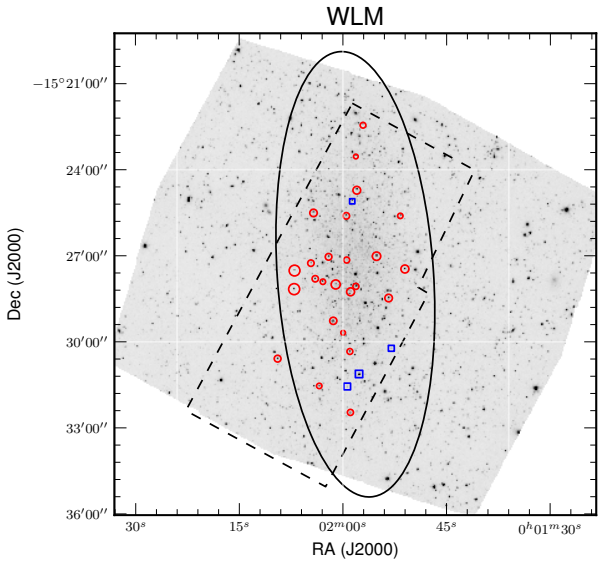

FIG. B3.— Figure B1 continued.